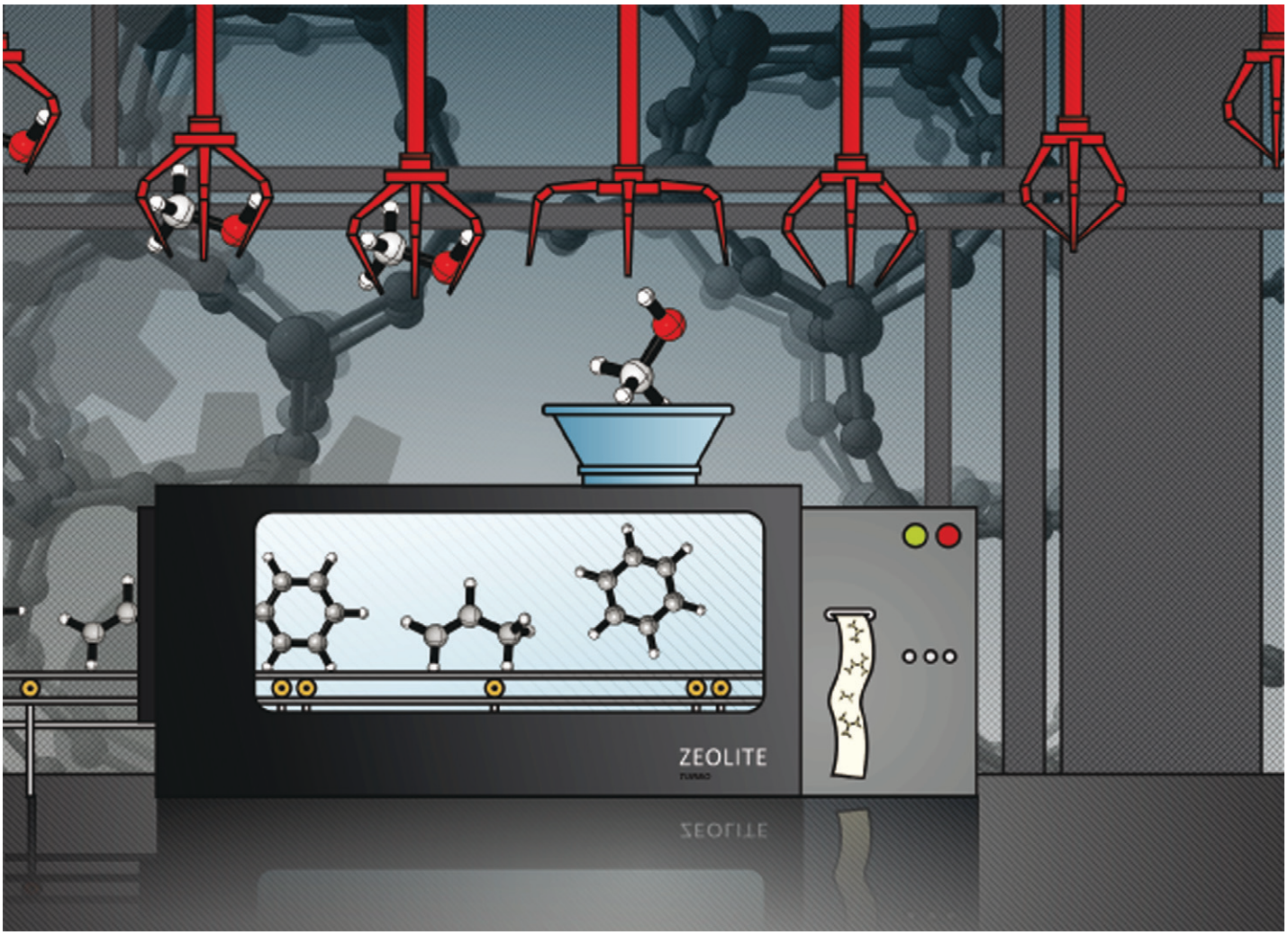


**Showcasing research from the Center for Molecular Modeling, Ghent University, Belgium**

Title: Towards molecular control of elementary reactions in zeolite catalysis by advanced molecular simulations mimicking operating conditions

Advanced *ab initio* molecular dynamics techniques enable study of the influence of catalyst topology and acidity, reaction temperature and the presence of additional guest molecules on methylation reactions of benzene and propene, which are crucial reaction steps in the conversion of methanol into hydrocarbons. Our advanced simulations provide detailed insight into how operating conditions impact the competition of the concerted and stepwise methylation mechanism and thus the reaction kinetics.

## As featured in:


See Veronique Van Speybroeck *et al.* *Catal. Sci. Technol.*, 2016, **6**, 2686.

ROYAL SOCIETY OF CHEMISTRY

www.rsc.org/catalysis

Registered charity number: 207890

Catalysis Science & Technology

PAPER

View Article Online
View Journal | View Issue



Cite this: *Catal. Sci. Technol.*, 2016, **6**, 2686

# Towards molecular control of elementary reactions in zeolite catalysis by advanced molecular simulations mimicking operating conditions†

Kristof De Wispelaere, Simon Bailleul and Veronique Van Speybroeck*

Zeolites are the workhorses of today's chemical industry. For decades they have been successfully applied, however many features of zeolite catalysis are only superficially understood and in particular the kinetics and mechanism of individual reaction steps at operating conditions. Herein we use state-of-the-art advanced *ab initio* molecular dynamics techniques to study the influence of catalyst topology and acidity, reaction temperature and the presence of additional guest molecules on elementary reactions. Such advanced modeling techniques provide complementary insight to experimental knowledge as the impact of individual factors on the reaction mechanism and kinetics of zeolite-catalyzed reactions may be unraveled. We study key reaction steps in the conversion of methanol to hydrocarbons, namely benzene and propene methylation. These reactions may occur either in a concerted or stepwise fashion, *i.e.* methanol directly transfers its methyl group to a hydrocarbon or the reaction goes through a framework-bound methoxide intermediate. The DFT-based dynamical approach enables mimicking reaction conditions as close as possible and studying the competition between two methylation mechanisms in an integrated fashion. The reactions are studied in the unidirectional AFI-structured H-SSZ-24, H-SAPO-5 and TON-structured H-ZSM-22 materials. We show that varying the temperature, topology, acidity and number of protic molecules surrounding the active site may tune the reaction mechanism at the molecular level. Obtaining molecular control is crucial in optimizing current zeolite processes and designing emerging new technologies bearing alternative feedstocks.

Received 30th November 2015,
Accepted 30th January 2016

DOI: 10.1039/c5cy02073e

www.rsc.org/catalysis



## 1. Introduction

Zeolites are prominent and versatile heterogeneous catalysts and chemical conversions in zeolites play an essential role in today's industrial catalysis.[1–3] In view of depleting oil reserves, an increasing demand for base chemicals and the development of more sustainable chemical processes, the industry is shifting towards alternative feedstocks such as natural gas, coal, biomass or waste. To allow conversion of non-conventional feedstocks there is a continuous search for more advanced zeolite structures, with a higher stability and ability to convert heavier feedstocks and molecules containing heteroatoms.[4–7] Although many zeolite-catalyzed processes have successfully been applied for several decades, many features of the materials and reaction mechanisms at the molecular scale are only superficially understood. With the intelligent molecular design of the optimal catalyst for a given process as the ultimate goal, more detailed molecular-level insights are a prerequisite. This is especially important to get track of elementary reactions at operating conditions, which is straightforward neither from experiment[8–10] nor from theory.[11,12]

In modern society, oil derivatives are ubiquitous in daily life. However, during the last decades, petrochemical industry suffers from unstable oil prices due to the waning oil reserves and political instabilities in oil producing countries in the Middle East. Moreover, due to an increasing world population and quality of living, the demand for energy and base chemicals increases exponentially. All these factors initiated the quest for processes to produce hydrocarbons starting from non-conventional feedstocks such as coal, natural gas or biomass, which resulted in a huge interest for the methanol to hydrocarbons (MTH), gasoline (MTG) and olefins (MTO) processes. In the last decades these processes have been commercialized.[13,14] UOP and Norsk Hydro (now INEOS), Total, Lurgi and the Dalian Institute of Chemical Physics (DICP) each developed their own version of the

*Center for Molecular Modeling (CMM), Ghent University, Technologiepark 903, B-9052 Zwijnaarde, Belgium. E-mail: veronique.vanspeybroeck@ugent.be*

† Electronic supplementary information (ESI) available. See DOI: 10.1039/c5cy02073e

process.[15–18] In view of the large availability of coal in China, many companies have taken up the DICP technology, resulting in a conversion capacity of more than ten million tons of methanol per year.

The MTH process also received a large interest from academia as its reaction mechanism is extremely complex, featuring many often competing reaction cycles at the same time. It has been found that the MTH catalyst has a supramolecular nature, meaning that next to the zeolite framework with its Brønsted acid site, also a hydrocarbon pool (HP) – these are organic molecules occluded in the zeolitic pores – co-catalyzes the reactions as schematically represented in Scheme 1.[13,19–21]

HP species can be subdivided into aromatic and aliphatic compounds and each compound co-catalyzes the MTH chemistry in distinct reaction mechanisms.[11,13,19–21] Aromatics can undergo side-chain growth by methylation in the side-chain mechanism or subsequent ring contraction and expansion reactions in the paring mechanism to form olefins (Scheme 2). In the autocatalytic alkene cycle the olefins undergo methylation and cracking reactions. Both catalytic cycles may exist next to each other, which is called the dual cycle concept.[22–24] Svelle *et al.* found that ethene is the primary product from the aromatic cycle, whereas propene and higher alkenes originate from the alkene driven cycle.[23] The operation of each catalytic cycle during methanol conversion seems to depend on process conditions such as reaction temperature, the nature and composition of the feed and the catalyst topology and acidity.[13,14,19,25,26] Note that each catalytic cycle is initiated by a methylation reaction (highlighted area in Scheme 2). Therefore, the influence of process conditions on methylation reactions is assessed in the current study (*vide infra*).

Given its complexity, studying the MTH process requires the application of a set of advanced experimental and theoretical methods that are able to unravel complex chemical conversions in nanoporous materials. Hence, teams of experimental and theoretical chemists and chemical engineers from all over the globe devote their research projects to unravelling the complex mechanism of the MTH process. Space – and time resolved spectroscopic techniques are nowadays able to image single particles and molecules[9,10,27] and kinetic measurements can yield information on isolated reaction steps.[28,29] Such kinetic information can at later instance be introduced in a micro-kinetic model to study the steady-state behavior of the process.[30–33] Also from a theoretical perspective many efforts to obtain profound understanding of the chemistry behind the MTH process have been performed and we refer the reader to some interesting reviews on this topic.[11,12]

Molecular modeling in heterogeneous catalysis has matured substantially and received a prominent role as molecular magnifying glass thanks to the development of advanced simulation tools and enormous investments in the ever increasing computer power.[11,12] State-of-the-art molecular modeling techniques are able to compute accurate adsorption enthalpies and rate coefficients of well-defined elementary reaction steps.[34–37] To date many theoretical studies rely on static optimization processes on the potential energy surface (PES), *i.e.* at 0 K, to which corrections can be applied to obtain enthalpic and entropic contributions at the actual reaction temperature.[11,38] The advantage of these techniques is that the most advanced and accurate electronic structure methods may be used to calculate the energy of the system.[11] However, this type of simulations only yields information on a restricted number of points on the PES, *i.e.* the reactant, transition state and product. Another class of simulation techniques consists of methods able to scan larger portions of the PES, hereby enabling to directly account for the dynamical behavior of the catalytic system at the actual reaction conditions. As such, one can account for temperature, pressure, additional guest molecules and the configurational freedom of the system. In this case one also has access to the free energy surface (FES) provided correct techniques are used to calculate the latter.[11,39,40] It should be emphasized that advanced molecular dynamics (MD) techniques to simulate catalytic reactions only recently entered the field of heterogeneous catalysis and their further exploration and application is ongoing.[11,41–54] The introduction of MD based techniques signified an important step towards more realistic models mimicking true reaction conditions. With the forthcoming molecular modeling results on reaction mechanisms, kinetics and thermodynamics it thus eventually becomes possible to impact and rationalize the choice of reaction conditions and the development of next generation MTH catalysts. In this view, MD based techniques are the methods of choice in this study and may give complementary insights.

One of the most investigated reaction steps in the framework of the MTH conversion is the methylation of alkenes and aromatics. These zeolite-catalyzed alkylation reactions are known to be crucial steps in the HP mechanism as they are responsible for carbon incorporation and growth of HP species (see Scheme 2).[55–62] However methylation reactions are also of a more general interest for industrial application to produce for example xylenes.[63] For methylation reactions, two mechanisms are known, being the concerted and stepwise pathway. The concerted mechanism starts from methanol physisorbed at the BAS and simultaneously forms the

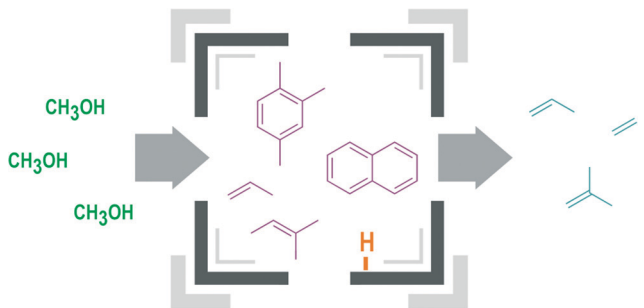


**Scheme 1** Schematic representation of the supramolecular nature of the MTH catalyst.[11] Reproduced with permission from The Royal Society of Chemistry.

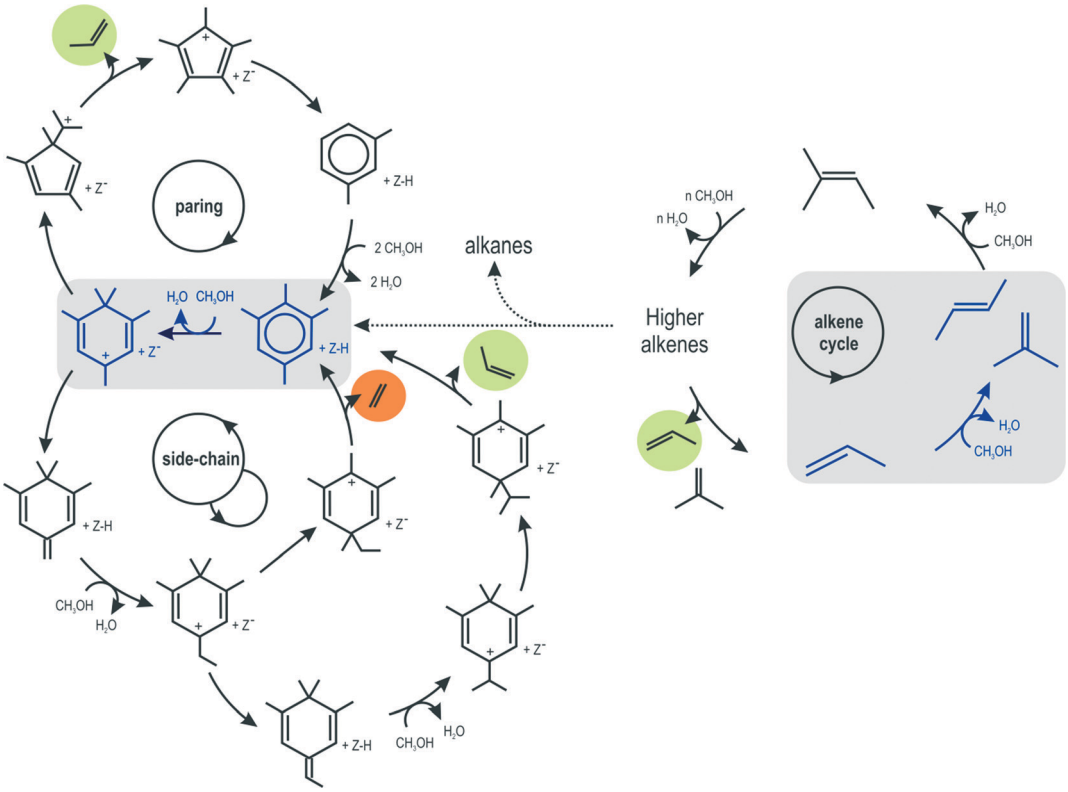


**Scheme 2** Overview of aromatic based and alkene based catalytic cycles for olefin formation during MTH conversion.[11] The shaded areas highlight the central role of methylation reactions in each catalytic cycle. Adapted with permission from The Royal Society of Chemistry.

methylation product and a water molecule. In the stepwise mechanism, on the other hand, methanol is dissociated into a framework-bound methoxide and a water molecule prior to the actual methylation. A compilation of the present knowledge on the reaction mechanism of zeolite-catalyzed methylations is given by Svelle *et al.*[29,64] Many theoretical studies available in literature assume the concerted methylation pathway,[28,35,36,56,62,65] however recent studies also account for the stepwise pathway.[21,59,66–70] Experimentalists, on the other hand, encounter major challenges to distinguish the concerted and stepwise methylation pathways.[29] Experimentally defined rate laws for methylation reactions typically exhibit a zeroth order methylation rate dependence on methanol partial pressure, irrespective of the reaction path.[60,61,71] Infrared and NMR measurements have demonstrated that surface-bound methoxides can be present during methylation reactions, indicating methylation might occur through the stepwise mechanism.[29] However, measurements at steady-state conditions indicate that the concerted pathway might prevail.[29] The mechanisms for benzene and propene methylation are shown in Scheme 3 and will be thoroughly investigated in this study.

Herein, some key aspects that have a distinct influence on the MTH conversion have been isolated and thoroughly investigated. Thereby we focused on two classes of influence factors, being (1) the influence of catalyst topology and acid strength and (2) process related factors being reaction temperature and the presence of additional guest molecules in

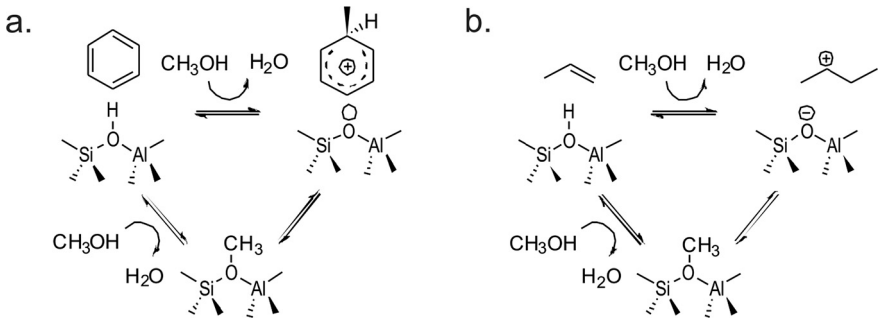


**Scheme 3** Concerted and stepwise pathways for the zeolite-catalyzed benzene (a) and propene (b) methylation reaction.

 

the reaction environment. An overview of the investigated influence factors is shown in Scheme 4. We selected benzene and propene methylation as case study since these are model compounds for the typical hydrocarbon pool species acting as co-catalysts during methanol conversion. This study more specifically aims at understanding how some operating conditions may tune the competition between a concerted and stepwise methylation reaction as schematically drawn in Scheme 4.

In this study, we consider two zeolite topologies characterized by one-dimensional pores of different sizes, namely the AFI and TON topology (Scheme 5). The similar shape and differing size enables to straightforwardly study the influence of confinement. For the AFI topology, we consider H-SSZ-24 and H-SAPO-5. Because of their different chemical composition, both frameworks exhibit different acid strength. Further, we study the influence of an additional methanol molecule surrounding the Brønsted acid site (BAS) to mimic different guest molecule loadings in the pores. Also the influence of temperature on the different reaction steps was studied.

The catalyst topology is an important factor during the methanol conversion process as it determines which HP species are active for olefin formation and thus the product selectivity as depicted in Scheme 5. In the one-dimensional pores of H-ZSM-22 only alkenes were found to be active HP species resulting in the production of branched $C_{5+}$ alkenes,[72–78] whereas aromatics were found to be dominating HP species in H-SAPO-34 and large pore zeolites H-beta and H-SSZ-24.[22,24,79–82] A high activity of aromatics is mostly coupled with a high selectivity towards ethene and propene. The role of catalyst topology has also extensively been studied for methylation reactions of alkenes and aromatics.[28,35,36,65] An optimal fit of the guest molecules in the zeolite pores seemed to be a determining factor for the reaction kinetics.[56] Next to reactivity, the catalyst topology and acidity were also found to impact diffusion rates of reaction products.[50,83,84]

Next to the catalyst's topology, also its acid strength plays a determining role for the activity of HP species. Studies with isostructural catalysts with different framework compositions and thus different acid strength show distinct behavior in terms of product selectivity and deactivation rate during methanol conversion.[53,82,86,87] Recently it has been

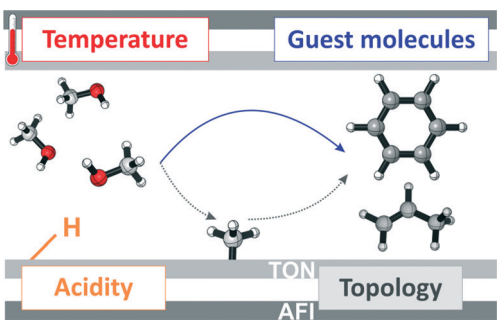


**Scheme 4** Overview of the influence factors on benzene and propene methylation investigated in this study.

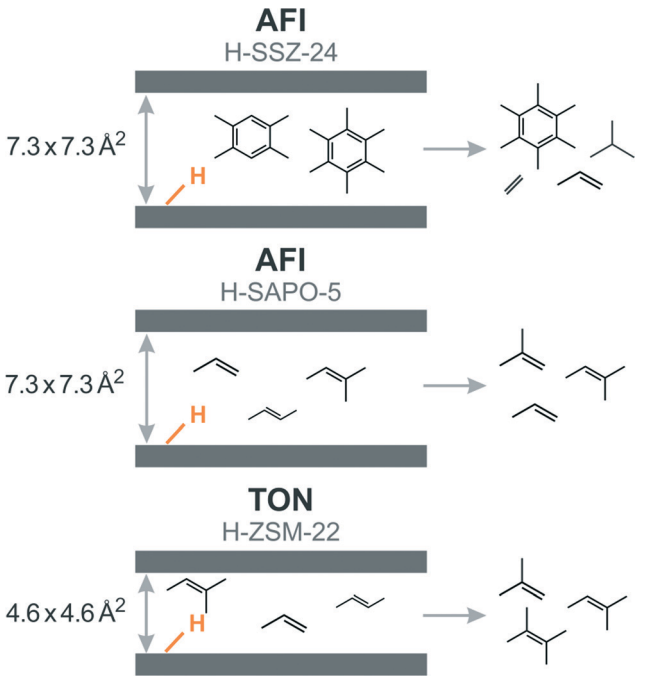


**Scheme 5** Schematic representation of the AFI-structured H-SAPO-5 and H-SSZ-24 catalysts and the TON-structured H-ZSM-22 zeolite, with indication of an acid site, the size of the pore opening (taken from the IZA database[85]) and the dominant hydrocarbon pool species and reaction products during methanol conversion.

demonstrated that the relative importance of the alkene and arene cycles can be tuned with acid strength in AFI materials.[53,82] While in the weaker acidic H-SAPO-5 the alkene cycle operates, aromatics are more important in the stronger acidic H-SSZ2-24. As a result, $C_{4+}$ alkenes are primary products in H-SAPO-5, whereas H-SSZ-24 mainly produces $C_{2-3}$ alkenes, aromatics and alkanes as depicted in Scheme 5.

On the side of process conditions, reaction temperature is a crucial parameter. Kinetic measurements and single event micro-kinetic modeling in H-ZSM-5 have demonstrated that the MTH product spectrum can be tuned by varying the reaction temperature.[30,88] Moreover, for methanol conversion in chabazite a combined operando UV-vis spectroscopy and online gas chromatography underlined the influence of temperature on the nature of active and deactivating species.[89] Methanol conversion over large-pore zeolites proceeds mainly *via* the arene cycle[22,24,80,81] but Iglesia and co-workers succeeded to promote the alkene cycle in large-pore materials by applying low temperatures and high pressures.[90,91] Also at the level of individual reaction steps, temperature has a major impact. The adsorption strength,[45,46] reaction kinetics and even the reaction mechanism depend on temperature. Recently Brogaard *et al.* applied a combined theoretical and experimental approach to study the various methylation pathways in ZSM-22,[32] revealing that alkene methylation proceeds *via* the stepwise mechanism (see Scheme 3) at typical MTH temperatures. A similar conclusion was recently drawn by Jones and Iglesia in a kinetic, spectroscopic and theoretical study,[92] showing that methoxy-mediated dissociative routes

become prevalent at higher temperatures and lower pressures due to a delicate balance between entropic and enthalpic effects. Van der Mynsbrugge *et al.* demonstrated after separating enthalpic and entropic barriers contributions to the free energy, that methoxide formation indeed involves a lower entropic barrier, compared to the direct methylation step.[12,52] This further gives evidence that the stepwise mechanism would be preferred at higher temperatures, due to favorable entropic effects. It thus becomes clear that disclosure of various competitive pathways may certainly not solely be based on potential energy profiles at 0 K. We refer the reader to the work of Gounder and Iglesia for a more in-depth discussion on the interplay between enthalpic and entropic effects.[93]

Finally, it should be noted that many theoretical studies assume the adsorption of a single methanol molecule per active site. This may hold under the conditions applied in experimental kinetic studies, which are typically performed at ambient pressure using dilute reagent streams at high feed rates to inhibit secondary reactions. However, under industrial MTH conditions, the conversion may occur at elevated pressures and temperatures.[94,95] Consequently, it might be important to take into account the presence of additional methanol molecules at the active site. It has been demonstrated earlier that the number of methanol molecules present at the BAS can influence the mechanism and kinetics of benzene methylation and methoxide formation in H-ZSM-5.[51,52]

Altogether, the zeolite-catalyzed MTH process is complex yet extremely versatile and by tuning some crucial process parameters, the process is able to meet the fluctuating market demands of ethene and propene. To obtain molecular control over the process, dedicated studies are indispensable to assess the influence of process conditions at the molecular level. Herein we show that state-of-the-art advanced MD techniques are able to describe the influence of catalyst and process related parameters on the mechanism and kinetics of methylation reactions. More specifically, we perform molecular dynamics and metadynamics simulations to assess the influence of catalyst's topology and acid strength, reaction temperature and the presence of additional methanol molecules at the active site on the reaction mechanism and kinetics of benzene and propene metylation reactions.

# 2. Materials and methods

## 2.1 Materials

Our simulations have been performed in the AFI-structured H-SSZ-24 and H-SAPO-5 and the TON- structured H-ZSM-22 catalysts. AFI catalysts are large pore materials characterized by one-dimensional 12 ring channels, whereas TON materials have smaller one-dimensional medium pores consisting of 10 rings as schematically represented in Scheme 5. For the AFI materials we considered both the aluminosilicate and silicoaluminophosphate version. The catalyst frameworks were represented by periodic models. For the AFI materials a $1 \times 1 \times 2$ super cell consisting of 48 T atoms has been used, whereas for the TON material a $1 \times 1 \times 3$ super cell consisting of 72 T atoms has been applied (see ESI† Fig. S1). Each catalyst model contains one BAS consisting of a substitutional defect (at the T1 position in the AFI topology and the T3 position in the TON topology) and a charge compensating proton. This corresponds with Si/Al ratios of 47 and 71 for H-SSZ-24 and H-ZSM22 and a (Al + P)/Si ratio of 47 for H-SAPO-5. The closest distances between two acid sites in the same channel were approximately 17 Å and 15 Å in the AFI and TON topologies and 14 Å between two acid sites in adjacent channels for both topologies. As such we can conclude that we modeled isolated acid sites. It has previously been reported that the rate per acid site of propene oligomerization over MFI type materials was affected by the acid site density up to Si/Al ratios of 40, but a further increase did not significantly affect the rate.[96] As the MD runs have been performed in the NPT ensemble (*vide infra*) the unit cell volume and parameters were variables during the simulations. Average cell volumes and parameters are listed in Table S1 of the ESI.†

## 2.2 *Ab initio* molecular dynamics

The behavior of guest molecules in the different catalysts is analyzed by density functional theory (DFT) based *ab initio* MD simulations. All DFT simulations have been performed with the CP2K software package[97,98] by using the combined Gaussian and Plane Wave (GPW) basis sets approach.[99,100] The revPBE functional was chosen for its improved performance for solid-state calculations relative to the commonly used PBE functional.[101] The DZVP-GTH basis set and pseudopotentials[102] were used, and Grimme D3 dispersion corrections[103] were added. To fully take the flexibility of the host frameworks and the dynamics of the guest molecules into account, simulations were carried out in the NPT ensemble at 250 °C or 350 °C and around 1 bar. During the *ab initio* MD simulations, the temperature was controlled by a chain of five Nosé–Hoover thermostats[104] and the pressure by an MTK barostat.[105] The time step for integration of the equations of motion was set to 0.5 fs. All systems were first equilibrated for 5 ps, followed by a production run of 50 ps. With our *ab initio* MD approach we only have access to relatively short time scales; however, these simulation times were sufficient to obtain convergence of the reported data (*vide infra*).

## 2.3 Metadynamics

Subsequently, metadynamics (MTD) simulations were performed in the NVT ensemble at 250 °C and 350 °C starting from equilibrated structures from the MD simulations. During the MTD simulations, the temperature is again controlled by a chain of five Nosé–Hoover thermostats. Furthermore, time-averaged cell parameters obtained from the NPT runs are used as constant values. These time-averaged cell parameters are summarized in Table S1.† The idea behind metadynamics calculations is that free energy wells are filled with Gaussian hills along a set of collective variables

 

(CV), here defined by coordination numbers (CN):

$$\mathrm{CN} = \Sigma_{i,j} \frac{1-\left(r_{ij}/r_0\right)^{nn}}{1-\left(r_{ij}/r_0\right)^{nd}} \quad (1)$$

where the sum runs over two sets of atoms $i$ and $j$, $r_{ij}$ is the distance between atoms $i$ and $j$ and $r_0$ represents the reference distance.[106] For all coordination numbers used in this study, a reference distance $r_0$ of 2.0 Å was chosen, because this value lies in the range of typical transition state distances of the bonds that have to be broken and formed during a methylation or methoxide formation. The parameters *nn* and *nd* are set to 6 and 12, respectively, ensuring a value of 0.5 for each CN term at the reference distance and fast decaying value at larger distances. Quadratic walls were used to restrict the simulations to an area of interest on the free energy surface (FES) (details are given in Fig. S2†). The reacting methanol molecule is kept close to the acidic proton and the free energy valley corresponding with the methylation product is not entirely sampled to prevent the formation of more stable cations and as such enhance barrier recrossings. The initial hills were 5 kJ mol$^{-1}$ high and after each barrier recrossing, the height of the added Gaussian hills is adequately halved to enhance the FES convergence until hills of 0.625 kJ mol$^{-1}$ are added. A new hill was spawned every 50 time steps. The width of all Gaussians was set to 0.02. The integration time step was set to 0.5 fs for all MTD simulations. Two sets of MTD simulations have been carried out and an overview of the studied reaction steps and applied CVs is given in Scheme 6. Initially, MTD simulations with three CVs starting from the co-adsorbed complexes were performed to directly sample the competition between the concerted and stepwise methylation mechanism. As such, the two sets of three reaction steps displayed in Scheme 3a and b were each sampled in one simulation, hereby using CN1, CN2 and CN3 (Scheme 6) to break methanol's C–O bond, form a new C–C bond or form a new C–O bond with the framework. As these simulations typically require very long simulation times to obtain converged free energy barriers, the 3D simulations were only used to extract information on which barrier was crossed first and thus which reaction exhibits the lowest free energy barrier. Next, for each system three MTD simulations applying two CVs were performed to determine accurate free energy barriers for the concerted and stepwise methylation steps. For the concerted methylation CN1 and CN2 as shown in Scheme 6 were applied. For the first and second step of the stepwise methylation, (CN1, CN3) and (CN3, CN2) were used as CVs, respectively. While simulating the formation of methoxides in these 2D simulations, the hydrocarbon molecule was assumed not to be co-adsorbed yet. Furthermore, the water molecule formed upon methoxide formation was assumed to be desorbed when sampling the methylation by a framework-bound methoxide.

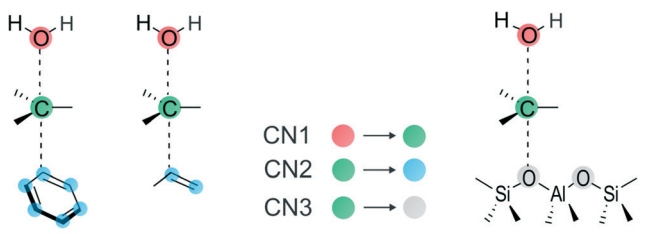


**Scheme 6** Schematic of the applied collective variables for the MTD simulations of benzene and propene methylation.

The MTD simulations with 2 CVs yield two-dimensional FESs. Consequently, a free energy barrier $\Delta G^{\ddagger}$ can be computed after projection of the 2D FES onto a 1D surface, taking the difference (CV2–CV1) as the reaction coordinate:

$$G(\mathrm{CV2}-\mathrm{CV1}) = -\frac{1}{\beta}\ln\left(\int_{-\infty}^{+\infty} d_{\mathrm{CV1}} \exp\left[-\beta G(\mathrm{CV2}-\mathrm{CV1},\mathrm{CV1})\right]\right) \quad (2)$$

Subsequently, the $\Delta G^{\ddagger}$ values can be calculated as the difference between the free energy of the transition state ensemble and the free energy of the reactant region on the obtained 1D FES:

$$\Delta G^{\ddagger} = -\frac{1}{\beta}\ln\frac{\exp\left[-\beta G(TS)\right]}{\int_{-\infty}^{TS}\exp\left(-\beta G(s)\right)\mathrm{d}s} \quad (3)$$

where $\beta = \frac{1}{k_{\mathrm{B}}T}$ with $k_{\mathrm{B}}$ the Boltzmann constant and TS is the position at the top of the barrier along the normalized reaction coordinate *s*. Analogously, the free energy of reaction $\Delta G_{\mathrm{r}}$ can be calculated by comparing the free energy in the product valley and reactant valley according to

$$\Delta G_{\mathrm{r}} = -\frac{1}{\beta}\ln\frac{\int_{TS}^{+\infty}\exp\left(-\beta G(s)\right)\mathrm{d}s}{\int_{-\infty}^{TS}\exp\left(-\beta G(s)\right)\mathrm{d}s} \quad (4)$$

In practice, the boundaries of the integrals in eqn (3) and (4) are not infinite, but −1 and +1 due to the definition of the 1D coordinate.

The reported free energies were calculated as the mean free energy over the part of the simulation where the barrier height starts to fluctuate around a mean value and the dynamics along the reaction coordinate become diffusive. The statistical errors were computed as the standard deviation of the mean after removal of correlated data values. The MTD simulations were continued until a statistical error lower than 5 kJ mol$^{-1}$ on the barrier height was obtained. This resulted in total simulation times varying between 50 and 140 ps. Note that due to the accelerating effect of the bias potential on the dynamics of the system, these simulation times do not have a physical meaning. Recently schemes have been developed to translate metadynamics back to regular

dynamics to calculate transition rates.[107] As we do not aim at calculating the most accurate free energy barriers and reactions free energies, our DFT-D approach gives enough insights to understand the observed trends. Moreover, the high computational cost of our dynamical approach hampers the application of higher level DFT methods[11,108] such as hybrid functionals (*e.g.* B3LYP or PBE0) or functionals including parametrization for dispersion interactions such as M06-2X developed by Truhlar,[109–112] ωB97X-D developed by Head-Gordon[113] or BEEF-vdw developed by Nørskov.[114]

Further, it is worth mentioning that in total 14 MD simulations, 14 MTD simulations with 3 CVs and 29 MTD simulations with 2 CVs have been performed. The total estimated calculation time on single 2 × 8 core Intel E5-2670 (Sandy Bridge) nodes was approximately 1350 nodedays.

### 2.4. Geometrical analysis

From the MD and MTD simulations, we extracted the orientation of the hydrocarbons in the channels throughout the simulations. Therefore, two angles – denoted as $\alpha$ and $\beta$ in the remainder of this article – were defined to uniquely define the orientation of benzene and propene in the AFI and TON channels. $\alpha$ was defined as the angle between the channel axis and the plane spanned by the six carbons atoms of benzene (Scheme 7a) or the plane spanned by the three carbon atoms of propene (Scheme 7b). $\beta$ was defined as the angle between a vector in a cross section of the channels, perpendicular to the O–H bond of the BAS, and the planes spanned by the carbon atoms of benzene or propene (Scheme 7c and d). Due to the definition of both angles and for symmetry reasons, $\alpha$ and $\beta$ can vary between 0° and 90°. The accessible ($\alpha$, $\beta$) range is furthermore restricted by the boundary condition that $\alpha + \beta =$ 90°, which also originates from the definition of both angles. The orientations of benzene and propene corresponding with the boundaries are shown in Scheme 8. It can be expected that a higher likelihood to adopt a configuration close to (90°, 0°) (Scheme 8c and f), the more accessible the hydrocarbon's π-electrons are for reaction with methanol (*vide infra*). When methoxides are present on the BAS, on the other hand, it can be anticipated that orientations close to ($\alpha$, $\beta$) values of (0°, 0°) (Scheme 8a and d) will be susceptible to reaction with a framework-bound methoxide.

From the MD simulations, also two reactivity indices were calculated which relate to the relative position of the methylating agent and the hydrocarbon with respect to each other and the position of methanol with respect to the BAS. A similar approach was followed in ref. 53. The probability of methanol protonation was calculated as the probability that the O–H interaction distance between methanol's oxygen atom and the proton of the BAS is smaller than 1.2 Å. This index merely represents the intrinsic reactivity of the methanol molecule as it needs to get protonated in any reactive event. To calculate the probability to form a pre-reactive complex between methanol and benzene or propene, three criteria were tested. First, the orientation of methanol and the

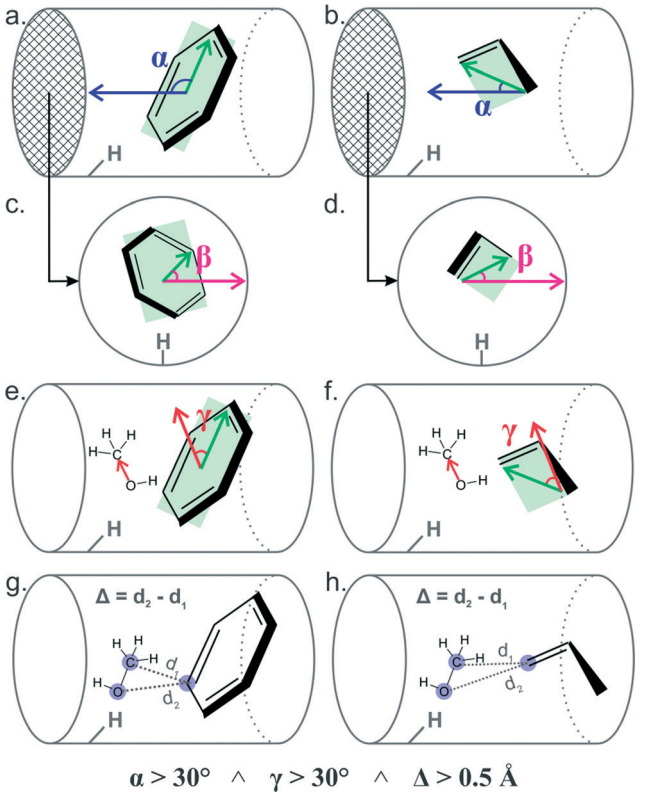


**Scheme 7** Schematic representation of the calculated angles between the plane spanned by the carbon atoms of benzene or propene and (a,b) the channel axis ($\alpha$), (c,d) the channel cross-section ($\beta$) and (e,f) the methanol C–O bond ($\gamma$) during the set of MD simulations. (g–h) Difference Δ of distances $d_2$ and $d_1$ between methanol and benzene or propene.

hydrocarbon with respect to each other has to be favorable, meaning that the methyl group has to point towards the hydrocarbon to enable the methyl transfer. This was expressed by a distance and angle criterion. The distance difference Δ (Scheme 7g and h) between the shortest O–C distance between methanol and the hydrocarbon ($d_2$) and the shortest C–C-distance between methanol and the hydrocarbon ($d_1$) had to exceed 0.5 Å. Additionally, an angle $\gamma$ was introduced to trace the angle between the methanol C–O bond and the plane spanned by the hydrocarbon's carbon atoms (Scheme 7e and f). The angle $\gamma$ can range from 0° to 90° and both boundaries are presented in Scheme 8g–j for co-adsorbed benzene and propene. The C–O bond was considered to adopt a favorable orientation with respect to the hydrocarbon when $\gamma$ exceeded the cut-off value of 30°. Finally, also the orientation of the hydrocarbon within the channel has to be favorable to enable the methylation reaction. Indeed, methyl transfer can only take place when the π-electrons of the double bond(s) to which it will attach are accessible for the methyl group. From Schemes 7 and 8 it can be seen that this is the case when $\alpha$ is not too close to zero. Therefore we selected a cut-off value for $\alpha$ of 30°. The full criterion for pre-reactive complex formation was then $\Delta > 0.5$ Å, $\alpha > 30°$ and $\gamma > 30°$.

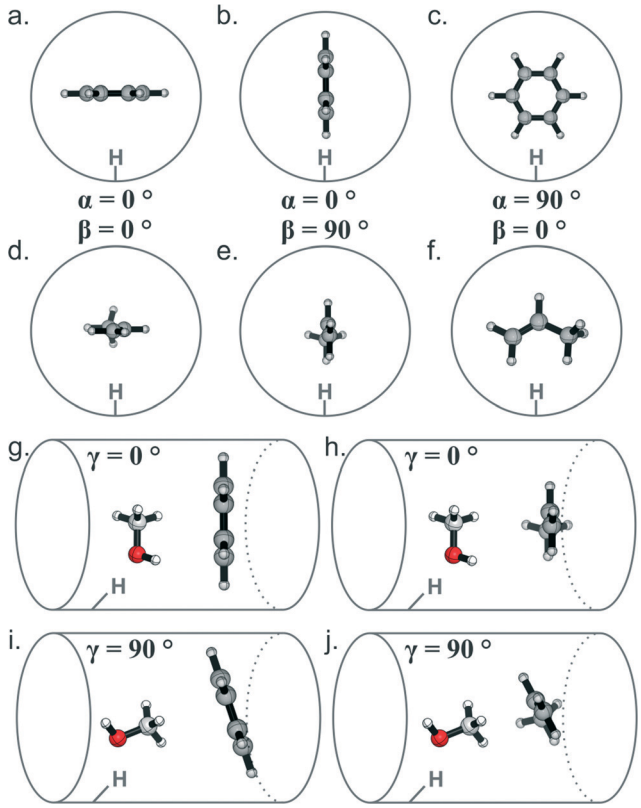


**Scheme 8** Orientations of benzene (a–c) and propene (d–f) corresponding with the boundaries of the accessible ($\alpha$, $\beta$) range in a one-dimensional zeolitic channel with indication of the $\alpha$ and $\beta$ values; orientations in which methanol and benzene (g) or propene (h) are not pointing towards each other ($\gamma$ = 0°) and orientation in which methanol and benzene (i) or propene (j) do point towards each other ($\gamma$ = 90°).

## 3. Results and discussion

By performing advanced MD simulations we aim at obtaining insights into the impact of catalyst topology and acidity, reaction temperature and the presence of additional protic guest in the reaction environment on methylation reactions of benzene and propene under MTH conditions. Therefore, the first goal of this study was to investigate the dynamic behavior and mobility of the reactants for benzene and propene methylation by a detailed MD study. For this purpose, we determined the most probable co-adsorption complexes of methanol with benzene or propene in a detailed MD study and attempted to link these observations with the actual reactivity for the concerted and stepwise methylation reactions.

### 3.1 Co-adsorption of reactants for benzene and propene methylation

A first set of MD runs comprises simulations of methanol with co-adsorbed benzene or propene in H-SSZ-24, H-SAPO-5 and H-ZSM-22 at 250 °C and 350 °C and around ambient pressure. A first analysis of these runs consists of a thorough assessment of the orientation of the hydrocarbons in the one-dimensional zeolitic pores using the angles $\alpha$ and $\beta$ as defined in Schemes 7 and 8. For each state sampled during the MD runs, the values for $\alpha$ and $\beta$ have been calculated. The resulting normalized 2D histograms are shown in Fig. 1 and snapshots corresponding with the (0°, 0°), (0°, 90°) and (90°, 0°) boundaries are displayed in Fig. 2.

From Fig. 1a it seems that benzene is relatively mobile in the AFI channels of H-SSZ-24 at 350 °C as almost the entire accessible ($\alpha$, $\beta$) area has been sampled during a 50 ps simulation. It can also be observed that benzene preferentially adopt an orientation with its plane facing the pore aperture, *i.e.* a structure resembling snapshot 3 in Fig. 2a with ($\alpha$, $\beta$) = (90°, 0°) as suggested by the hotspot indicated by the white arrow in the bottom-right part of Fig. 1a. The snapshot corresponding with this hotspot as displayed in Fig. 3a suggests that with such orientation, the π-electrons of the benzene ring are optimally accessible for methyl transfer from methanol during a methylation reaction. When the temperature for the same system is decreased to 250 °C, benzene becomes slightly less mobile and the preference for favorable structures for methylation in the bottom-right part of the ($\alpha$, $\beta$) plane becomes more pronounced as seen in Fig. 1c. A similar analysis was performed for co-adsorbed propene and it was found that propene is slightly more mobile than benzene in H-SSZ-24 (Fig. 1b and d). The preferential orientation of propene is similar to the one of benzene (Fig. 3b) meaning that also propene's π-electrons of the double bond are likely to be accessible for methyl transfer from methanol during a methylation reaction in H-SSZ-24.

When looking at the results for the AFI-structured H-SAPO-5 material at 350 °C (Fig. 1e and f), one can observe that an even larger range of ($\alpha$, $\beta$) combination has been sampled compared to H-SSZ-24. This might be related with the slightly larger pore size. Indeed, Table S1† shows that the time-averaged super cell volume of H-SAPO-5 is approximately 3% higher than for H-SSZ-24. Consequently, more configurations resembling snapshots 1 and 2 in Fig. 2a and b have been visited compared to H-SSZ-24. Fig. 1e and f display some hotspots indicated by the white arrows for the co-adsorbed complexes, but the normalization of the histograms reveals that in H-SAPO-5 there is a less pronounced preferential orientation of benzene and propene molecules in this less acidic AFI material. This suggests that the slightly larger pore diameter and lower acid strength induce weaker interactions between benzene or propene and the channel walls. This has been confirmed by calculated energies of interaction listed in Table S2.† That benzene interacts stronger with the SSZ-24 framework than with $AlPO_4$–5 was previously reported in an experimental and theoretical adsorption study of McCullen *et al.*[115] Fig. 3c and d displays snapshots corresponding with the co-adsorption hotspots for benzene and propene.

Just as in H-SSZ-24, the hotspots in the orientation histograms become more pronounced for benzene and propene in H-SAPO-5 at 250 °C (Fig. S3†). The multitude of sampled co-adsorbed complexes in the AFI materials gives a first

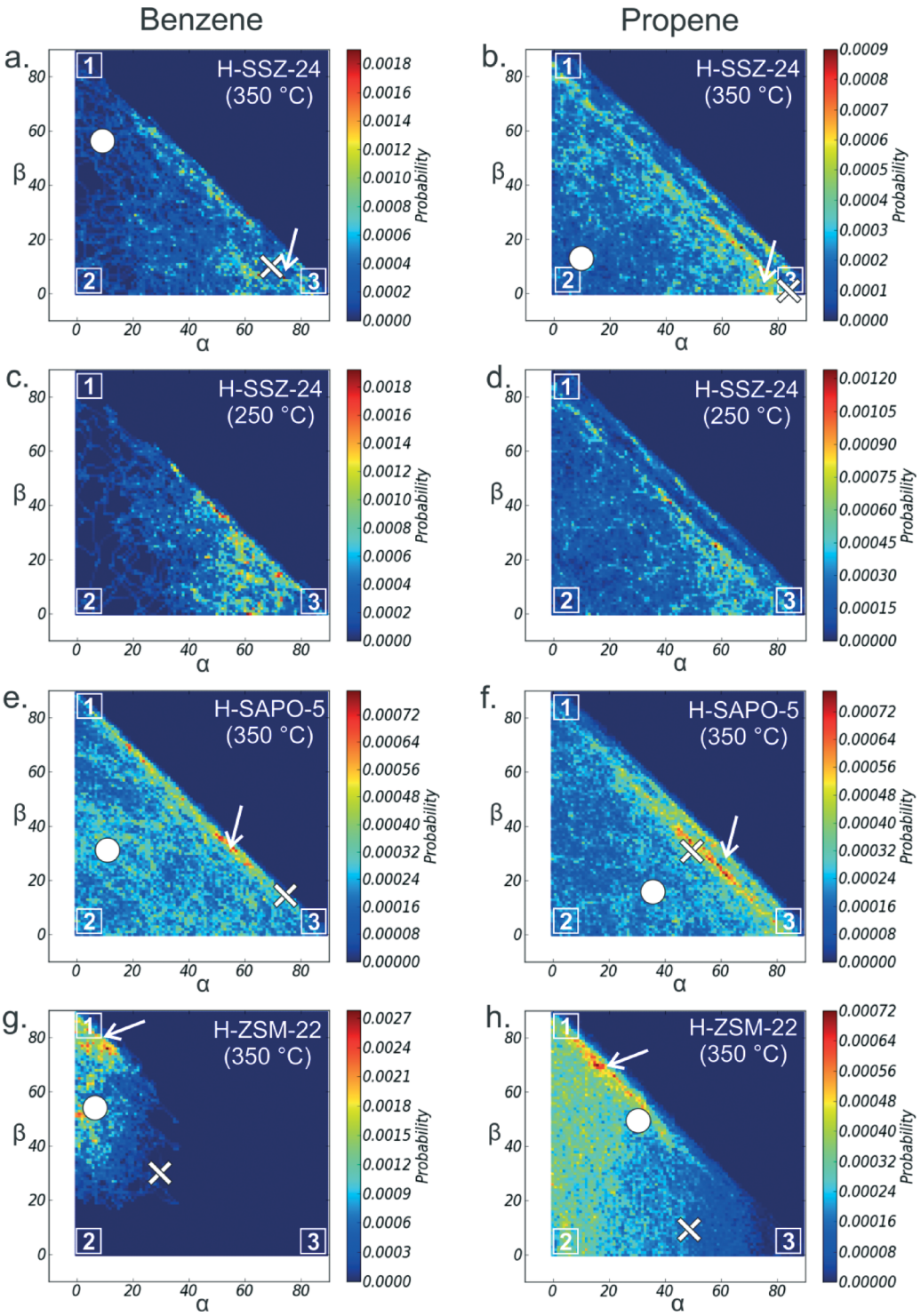


**Fig. 1** Two-dimensional normalized histograms displaying the orientation of co-adsorbed benzene and propene in H-SSZ-24 (a–d), H-SAPO-5 (e,f) and H-ZSM-22 (g,h) at 250 °C and 350 °C during a 50 ps MD simulation around ambient pressure and with one methanol molecule. The white arrows indicate the hotspots displayed in Fig. 3, the cross and circle the transition points for methylation by methanol and a methoxide as shown in Fig. 5.

indication of the complexity of the underlying potential and free energy surfaces for further methylation reactions.

Finally, the influence of the channel size was assessed by considering the TON-structured H-ZSM-22 catalyst. Fig. 1g clearly shows that benzene's mobility is severely hampered in this 10-ring channel and that benzene now preferentially co-adsorbs with its plane aligned with the channel axis as shown by the high probability to find benzene in a

 

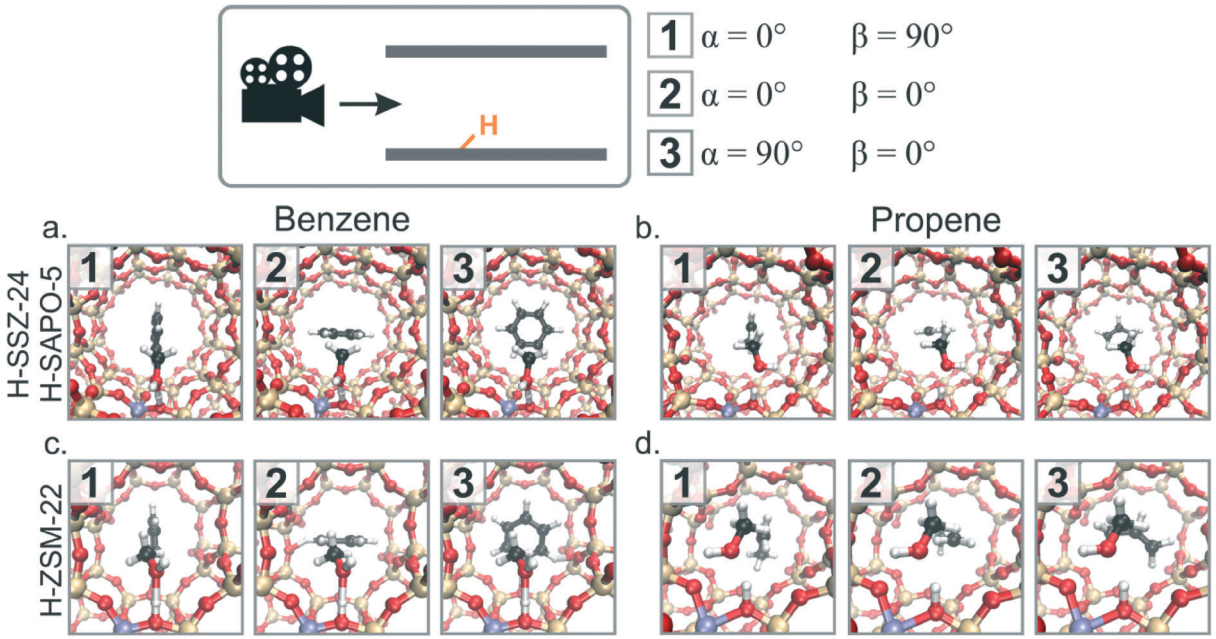


**Fig. 2** Snapshots at the boundaries of the accessible ($\alpha$, $\beta$) area for co-adsorbed benzene and propene in the isostructural H-SSZ-24 and H-SAPO-5 materials (a,b) and the TON-structured H-ZSM-22 material (c,d) from MD simulations with one methanol molecule at 350 °C and around ambient pressure.

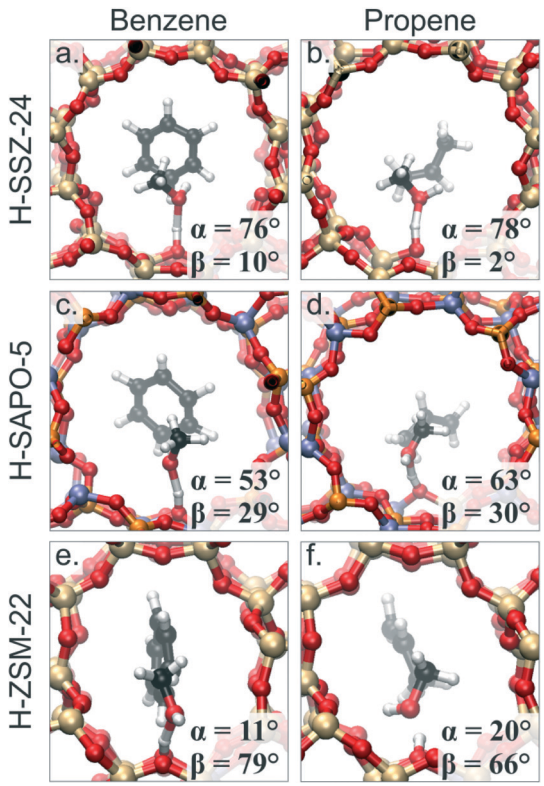


**Fig. 3** Snapshots of the most probable co-adsorption complexes of benzene and propene in H-SSZ-24 (a,b), H-SAPO-5 (c,d) and H-ZSM-22 (e,f) from MD simulations at 350 °C and around ambient pressure. The values of $\alpha$ and $\beta$ are indicated.

configuration with ($\alpha$, $\beta$) = (0°, 0°) (cfr. snapshot 1 in Fig. 2c). In this case, benzene's $\pi$-electrons are less accessible for further reaction as also seen in Fig. 3e. Propene, on the other hand, exhibits a much higher mobility in H-ZSM-22 (Fig. 1h) and is thus expected to be more reactive towards methylation than benzene.

Furthermore, Fig. 1 displays the orientations of benzene and propene adopted during the first barrier crossing of the concerted methylation (indicated by the cross) and stepwise methylation (indicated by the circle) as sampled during the MTD simulations at 350 °C (see section 3.3). The proximity of the co-adsorption hotspots indicated by the white arrows and orientation for the concerted methylation for benzene and propene in H-SSZ-24 and propene in H-SAPO-5 makes us expect a high reactivity towards these reaction steps. In H-ZSM-22, on the other hand, it can be anticipated that methylation by a methoxide will be more reactive than by methanol.

To assess the influence of an additional methanol molecule on the co-adsorption behavior prior to methylation we also performed simulations of benzene and propene with 2 methanol molecules in H-SSZ-24 and H-SAPO-5 at 350 °C. We observed that an additional methanol molecule did not significantly alter the preferential orientation of the co-adsorbed hydrocarbons as seen in Fig. S4.†

From a detailed analysis of the orientation of benzene and propene co-adsorbed with methanol it can be concluded that catalyst topology, acid strength and reaction temperature substantially influence the mobility and preferential orientation of co-adsorption complexes for benzene and propene

methylation. The presence of an additional methanol molecule only has a minor influence. The snapshots depicted in Fig. 3 correspond to the hotspot regions in Fig. 1 and thus represent the most probable co-adsorbed complexes. Between H-SSZ-24 and H-SAPO-5, some differences can be noted between the orientations of benzene and propene in these most probable co-adsorbed complexes, which are originating from weaker interactions between the hydrocarbon guest molecules and the H-SAPO-5 framework. In H-ZSM-22, on the other hand, significantly different orientations were adopted compared to the AFI catalysts due to severe confinement effects. This effect is more pronounced for benzene than for propene. The medium-pore zeolite H-ZSM-22 severely restricts the mobility of guest molecules like benzene and propene compared to the large-pore AFI materials, which is expected to have implications on the kinetics and mechanism of methylation reactions.

### 3.2 Reactivity indices from MD

The preceding discussion pointed towards some more or less reactive configuration of the reactants for methylation in the ($\alpha$, $\beta$) space. In this section, we explicitly study some reactivity indices computed from the MD trajectories as introduced in section 2.4. These indices correspond to favorable orientations of methanol and benzene or propene with respect to each other for methylation reactions. The indices were defined as the probability that methanol is protonated and the probability that methanol and the hydrocarbon form a pre-reactive complex for direct methylation according to the concerted pathway. Fig. 4 displays these two indices for propene and benzene co-adsorbed with one methanol molecule in H-SSZ-24, H-SAPO-5 and H-ZSM-22 at 250 and 350 °C.

In Fig. 4 the impact of three factors as presented in Scheme 3 becomes clear, *i.e.* catalyst acidity, topology and reaction temperature. The results show a clear clustering per material, indicating that acid strength and topology significantly influence these indices and thus the reactivity towards direct methylation. The probability to protonate methanol during the 50 ps MD runs increases in the order H-SAPO-5 < H-SSZ-24 < H-ZSM-22. This quantity is directly related to the acid strength of the studied materials and this trend follows the order of acid strength. Indeed, an analysis of the acidic hydroxyl group's bond length shows that H-SAPO-5 is the weakest acid, whereas the zeolites H-SSZ-24 and H-ZSM-22 have a similar acid strength (Fig. S5†). Due to the smaller pores of H-ZSM-22, protonated methanol can be more efficiently stabilized, which might explain the higher probability for methanol protonation compared to H-SSZ-24. Note that many measures for acidity of solid acids are available based on *e.g.* IR spectra and adsorption enthalpies.[116,117] Acid strength also seems to influence the relative reactivity of propene and benzene in the two isostructural AFI materials. Where benzene is more likely to form pre-reactive complexes for methylation in the more acidic H-SSZ-24 material, propene exhibits the highest probability to form favorable co-adsorbed complexes in H-SAPO-5. This is in line with what was earlier reported.[53]

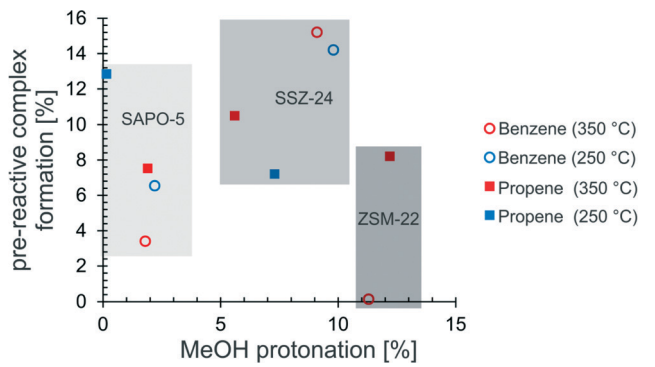


Fig. 4 Probability of methanol protonation and formation of a pre-reactive complex for benzene and propene methylation with one methanol molecule in H-SAPO-5, H-SSZ-24 and H-ZSM-22 at 250 °C (blue symbols) and 350 °C (red symbols).

In H-ZSM-22, propene is able to adopt conformations resembling pre-reactive complexes, but for benzene this is not the case as indicated by the nearly zero probability to form pre-reactive complexes for benzene. Here, the topological effect is clearly visible. According to Fig. 1g, the confined space in the 10-rings of H-ZSM-22 severely limits the mobility of a benzene molecule. Fig. 4 now reveals that this prohibits the spontaneous formation of favorable co-adsorbed complexes for methylation. The most probable co-adsorption complexes of methanol and benzene or propene shown in Fig. 3e and f already revealed that in these most probable configurations, the $\pi$-electrons of the hydrocarbons are not easily accessible for reaction with methanol.

The reaction temperature mainly impacts the vertical axis in Fig. 4. In H-SAPO-5, an increased temperature induces a lower probability to find a favorable co-adsorbed complex, whereas the reverse was found in H-SSZ-24. This can be attributed to a different temperature dependence of geometrical parameter $\Delta$ (Scheme 7g and h) in both AFI materials. While the probability that $\alpha$ and $\gamma$ are larger than 30° only slightly decreases with increasing temperature, the probability that $\Delta$ is larger than 0.5 Å increases in H-SSZ-24 and decreases in H-SAPO-5 (Fig. S6 and Table S3†). As this different temperature behavior is not straightforwardly reflected in the calculated free energy barriers (*vide infra*), it is hypothesized that our reactivity indices are not robust enough to properly distinguish between the two applied temperatures.

A similar analysis has been performed for the simulations of benzene with an additional methanol molecule. Addition of a methanol molecule to the co-adsorbed methanol–benzene system results in the formation of (protonated) hydrogen bonded clusters of the protic molecules which was found to mainly affect the reactivity index concerning methanol protonation. In H-SSZ-24 we found a 82% chance to find a methanol dimer, whereas this probability was only 27% in H-SAPO-5. For co-adsorbed benzene in H-SSZ-24 at 350 °C, the probability for methanol protonation increased from 9% for

 

a single methanol molecule at the BAS to 47% for two methanol molecules. Under the same conditions in H-SAPO-5, these probabilities were 2% and 10%. These results show that two methanol molecules more likely deprotonate the BAS prior to reaction than a single methanol molecule. These results correspond with earlier findings from theoretical studies applying static and dynamical approaches, stating that two methanol molecules are able to deprotonate the BAS in zeolitic catalysts.[49,118–122] Even if an additional methanol molecule is present, the lower acid strength of H-SAPO-5 as compared to H-SSZ-24 is still reflected in the relatively low probabilities to protonate methanol.

A convergence check of the calculated probabilities confirmed that the 50 ps MD simulations give sufficient sampling to obtain reliable results concerning co-adsorption behavior (see Fig. S7 of the ESI†).

Our simulations show that catalyst topology, acidity, reaction temperature and presence of an additional protic molecule have an important influence on the tendency to form protonated methanol and the probability to form a co-adsorbed complex for direct methylation in which the methyl group points towards the hydrocarbon and thus interacts with the π-electrons of its double bond(s). Based on these indices, it is expected that benzene and propene in H-SSZ-24, propene in H-SAPO-5 and propene in H-ZSM-22 will exhibit a high reactivity for the concerted methylation at 350 °C. In the next section these insights based on the dynamic co-adsorption behavior and mobility of guest molecules in the zeolite pores will be coupled to intrinsic free energy barriers for methylation.

### 3.3 Influence of reaction conditions on the free energy barriers for methylation

**3.3.1 Catalyst topology, acidity and reaction temperature.** After the MD simulations, metadynamics simulations were carried out to explicitly sample the reactive events. This allows to directly assess the impact of the factors listed in Scheme 4, *i.e.* zeolite topology and acidity, reaction temperature and presence of an additional guest molecule on the mechanism and free energy barriers for benzene and propene methylation. Hereby, we aimed at correlating the intrinsic reactivity from the MTD simulations with the in depth analysis of co-adsorbed complexes from the MD simulations and in particular the preferred orientation of co-adsorbed complexes or so-called hotspots (Fig. 1 and 3). As mentioned before, it is known that methylation reactions occur either in a concerted or stepwise fashion (see Scheme 3) and the MTD study specifically focused on the governing reaction mechanism.

We started the MTD simulations from equilibrated structures of the MD simulations of benzene or propene co-adsorbed with a single methanol molecule. Initially, explorative MTD simulations employing three collective variables were performed as sketched in Scheme 6 to obtain insights into the competition of the concerted and stepwise pathways when all molecules are adsorbed. The advantage of such MTD simulation is that it enables simulating competitive pathways in one run under the same conditions. As the MTD algorithm in principle first crosses the lowest free energy barrier, we can as such obtain information on the lowest activated mechanism by inspecting which barrier has been crossed first. For all simulations with one methanol molecule, it seemed that the concerted reaction step is the lowest activated step when all molecules are adsorbed in the system. At 350 °C methoxide formation has been sampled later in the simulation for all systems, whereas methoxide formation was never sampled at 250 °C during the 3D MTD simulations. This already indicates that the stepwise mechanism becomes a viable pathway at relatively high temperatures, which has been related with an entropic effect in earlier studies.[32,92]

To calculate free energy barriers, a set of 2D simulations was carried out for all systems. The resulting intrinsic free energy barriers and free energies of reaction for the concerted ($\Delta G^{\ddagger}_{\text{concerted}}$) and stepwise ($\Delta G^{\ddagger}_{\text{step1}}$, $\Delta G_{\text{r,step1}}$ and $\Delta G^{\ddagger}_{\text{step2}}$) benzene and propene methylations with one methanol molecule at 350 °C and 250 °C in H-SSZ-24, H-SAPO-5 and H-ZSM-22 are listed in Table 1, the corresponding FESs are displayed in Fig. S8–S11.† It was assumed that methoxide formation is not influenced by the hydrocarbon guest molecule and as such, only one set of $\Delta G^{\ddagger}$ and $\Delta G_{\text{r}}$ values is reported for methoxide formation per material and per temperature. Note that the aim was not to calculate the most accurate free energy barriers; instead we wanted to observe important trends related to the process conditions we are investigating in this study. To obtain barriers near chemical accuracy, other techniques need to be applied which are computationally extremely demanding. Such methods may be used for benchmark purposes on a selected set of reactions as was done in the work of Svelle and co-workers[35] and Göltl and co-workers.[45,123] Furthermore for AFI type materials under study here, it was shown by the present authors that not one single transition state exists, but rather a transition state ensemble which may be quite broad.[49] For ZSM-22, Brogaard found better defined transition states and in this case static methods might be employed as well.[32]

From the results for benzene and propene methylation in H-SSZ-24 at 350 °C it is clear that a concerted methylation is preferred over a methoxide formation, which is consistent with what was seen during the explorative 3D metadynamics simulations (*vide supra*). Indeed, the intrinsic free energy barriers for the concerted pathways (134 ± 3 and 123 ± 2 kJ mol$^{-1}$ for benzene and propene, respectively) are significantly lower than the free energy barrier for methoxide formation (160 ± 3 kJ mol$^{-1}$). Moors *et al.* calculated that the concerted benzene methylation in H-ZSM-5 at 400 °C exhibits a free energy barrier of only 118 ± 5 kJ mol$^{-1}$.[51] The higher value of 134 ± 3 kJ mol$^{-1}$ obtained here for H-SSZ-24 at 350 °C can be attributed to a more optimal fit of the reacting molecules in the MFI channel intersections than in the large AFI pores.[56] Methylations by methoxides under these conditions seem to be only slightly higher activated (137 ± 2 and 132 ± 1 kJ mol$^{-1}$ for benzene and propene, respectively) compared to the

**Table 1** Free energy barriers and reaction energies in kJ mol$^{-1}$ for the concerted ($\Delta G^{\ddagger}_{concerted}$) and stepwise methylation ($\Delta G^{\ddagger}_{step1}$, $\Delta G_{r,step1}$, $\Delta G^{\ddagger}_{step2}$) for benzene and propene with 1 methanol molecule at 250 °C and 350 °C in H-SSZ-24, H-SAPO-5 and H-ZSM-22. Values for propene methylation in H-ZSM-22 at 400 °C between parenthesis were taken from Brogaard et al[32]

| | | | Concerted | Stepwise | | |
|---|---|---|---|---|---|---|
| | | | $\Delta G^{\ddagger}_{concerted}$ (kJ mol$^{-1}$) | $\Delta G^{\ddagger}_{step1}$ (kJ mol$^{-1}$) | $\Delta G_{r,step1}$ (kJ mol$^{-1}$) | $\Delta G^{\ddagger}_{step2}$ (kJ mol$^{-1}$) |
| H-SSZ-24 | Benzene | 350 °C | 134 ± 3 | 160 ± 3 | 46 ± 4 | 137 ± 2 |
| | | 250 °C | 136 ± 1 | 179 ± 3 | 48 ± 4 | 127 ± 1 |
| | Propene | 350 °C | 123 ± 2 | 160 ± 3 | 46 ± 4 | 132 ± 1 |
| | | 250 °C | 118 ± 1 | 179 ± 3 | 48 ± 4 | 152 ± 3 |
| H-SAPO-5 | Benzene | 350 °C | 156 ± 1 | 162 ± 3 | 3 ± 1 | 130 ± 1 |
| | | 250 °C | 165 ± 4 | 180 ± 5 | 18 ± 5 | [a] |
| | Propene | 350 °C | 128 ± 5 | 162 ± 3 | 3 ± 1 | 127 ± 1 |
| | | 250 °C | 131 ± 1 | 180 ± 5 | 18 ± 5 | 152 ± 2 |
| H-ZSM-22 | Benzene | 350 °C | 151 ± 2 | 148 ± 3 | 31 ± 2 | 124 ± 3 |
| | Propene | 350 °C | 115 ± 1 (122) | 148 ± 3 (158) | 31 ± 2 (1) | 101 ± 1 (65) |

[a] No converged value could be obtained.

concerted reaction with methanol. A similar intrinsic reactivity of methanol and methoxides was also reported by Van der Mynsbrugge *et al.* and Brogaard *et al.* for alkene methylation in H-ZSM-5 and H-ZSM-22 with a static DFT approach.[32,52]

When comparing the intrinsic free energy barriers for benzene and propene at 350 °C, it seems that propene methylation is lower activated than benzene methylation by approximately 11 kJ mol$^{-1}$. Experimentally measured rates however show that benzene methylation occurs faster than propene methylation in H-SSZ-24 at 350 °C.[53] However, experimentally one measures the apparent kinetics, hence direct comparison with our intrinsic reactivity study is not possible. Moreover, Brogaard and co-workers stressed that it is in general not possible to compare calculated apparent activation energies of methylation reactions with values obtained from steady-state kinetic experiments.[32] Calculation of apparent free energy barriers and kinetics requires the determination of the reaction order for each reactant to construct a rate expression and subsequently the accurate determination of adsorption and co-adsorption free energies. This is however beyond the scope of this work.

When the temperature is lowered to 250 °C, the differences between the free energy barriers for the concerted and stepwise methylations in H-SSZ-24 become more pronounced. The free energy barriers for the concerted benzene and propene methylations are not very sensitive to the applied temperature change as differences lie within the 5 kJ mol$^{-1}$ error margin of barriers calculated with DFT methods. This indicates that no major entropic effects are at play for this reaction mechanism. The free energy barrier for methoxide formation instead increased substantially (17 kJ mol$^{-1}$) with decreasing temperature, suggesting this reaction exhibits a considerable entropic barrier. This effect has in earlier studies been attributed to the intermediate release of a water molecule and attachment of the methyl group to the framework during methoxide formation.[32,92] Brogaard and co-workers pointed out that the stepwise mechanism for propene methylation in H-ZSM-22 becomes important at temperatures above 327 °C based on a combined study comprising TAP kinetic experiments, DFT calculation and micro-kinetic modeling.[32]

In the weaker acidic H-SAPO-5 catalyst, the concerted pathway also seems to dominate the benzene and propene methylation. Note however that in the case of benzene methylation a concerted methylation (156 ± 1 kJ mol$^{-1}$) and methoxide formation (162 ± 3 kJ mol$^{-1}$) at 350 °C are almost equally high activated, which is not the case for propene (128 + 5 kJ mol$^{-1}$ *versus* 162 ± 3 kJ mol$^{-1}$). The free energy barrier for the concerted benzene and propene methylations at 350 °C in H-SAPO-5 are respectively around 22 and 5 kJ mol$^{-1}$ higher than in H-SSZ-24. Intuitively, one would expect that a lower acid strength results in higher intrinsic free energy barriers; however benzene methylation seems to be much more sensitive to acid strength than propene methylation. A possible explanation has been proposed by Iglesia and co-workers, stating that transition states with localized charges are less sensitive to acid strength than those with diffuse charges.[124] It can indeed be expected that the positive charge on the transition state for propene methylation is more localized than for benzene, due to the conjugated π-system of the latter. The difference of 22 kJ mol$^{-1}$ between the $\Delta G^{\ddagger}_{concerted}$ values for benzene and propene methylation at 350 °C in H-SAPO-5 further show that the intrinsic reactivity towards methylation of propene is higher than benzene. Returning to the reactivity indices presented in Fig. 4, this might be related with the fact that propene is more likely to form pre-reactive complexes with methanol for methylation than benzene in H-SAPO-5.

In the context of the MTH process, these findings are in line with the experimental observation that in H-SAPO-5 the alkene cycle dominates product formation whereas aromatics are the main HP species during methanol conversion in H-SSZ-24.[53,82,87] To the best of our knowledge no direct experimentally derived kinetics are available for methylation reactions in the AFI topology. It should however be noted that the two reactivity indices extracted from MD, being methanol protonation and pre-reactive complex formation for methylation, were found to correlate well with experimentally

 

measured reaction rates for methylation at 350 °C. Benzene methylation was found to be much faster than propene methylation in H-SSZ-24, whereas both reactions occurred at similar rates in H-SAPO-5. So far, no experimentally defined free energies of activation have been reported.[53]

Methoxide formation does not exhibit a significant influence of acid strength, which can again be related with the rather localized positive charge on the methyl cation in the transition state (see ESI† section 10 for a further discussion). Furthermore, it seems that methoxides in H-SAPO-5 at 350 °C are much more stable with respect to the reactants than in H-SSZ-24 as can be seen from the largely differing $\Delta G_{r,step1}$ values in both materials, which can be related with the lower acid strength of the H-SAPO-5 framework. At 350 °C methoxides appear to be very reactive towards methylation in H-SAPO-5. When comparing the $\Delta G^{\ddagger}_{step2}$ values for benzene and propene H-SAPO-5 (130 ± 1 and 127 ± 1 kJ mol$^{-1}$) and H-SSZ-24 (137 ± 2 and 122 ± 1 kJ mol$^{-1}$) it can also be observed that methylation by a methoxide are not very sensitive to acid strength. In H-SAPO-5, the influence of lowering the temperature by 100 °C is similar as in H-SSZ-24.

Finally, a similar set of simulations has been performed in the H-ZSM-22 catalyst model. From the free energy barriers for benzene methylation at 350 °C is seems that the concerted pathway (151 ± 2 kJ mol$^{-1}$) and the first step of the stepwise pathway (148 ± 3 kJ mol$^{-1}$) are equally high activated, suggesting both mechanisms might be active at 350 °C in this material. That methylation of benzene with methanol in H-ZSM-22 exhibits relatively high $\Delta G^{\ddagger}$ values, despite the high acid strength, can be understood in view of the restricted mobility of benzene in the TON channels, inhibiting the formation of favorable pre-reactive complexes (see Fig. 1g and 4). For propene a high probability to form pre-reactive complexes for a concerted methylation step (Fig. 4) was found and this is clearly reflected in the relatively low free energy barrier $\Delta G^{\ddagger}_{concerted}$ (115 ± 1 kJ mol$^{-1}$). In Table 1 values in parentheses for propene methylation in H-ZSM-22 at 400 °C were taken from the work of Brogaard *et al.*, in which a static periodic BEEF-vdw approach was applied. There is a relatively good agreement between those results and our dynamical revPBE-D3 free energy barriers for concerted methylation and methoxide formation at 350 °C. Our calculations show that methoxides are less stable with respect to physisorbed methanol and also less reactive towards methylation of propene, compared to the results of Brogaard *et al.* For ZSM-22 transition state valleys are less broad and a relatively good correspondence between static and dynamic approaches may be expected, as observed here. Indeed, in terms of hydrocarbon orientation, the ensemble of transition states sampled with metadynamics in H-ZSM-22 is less broad than in the AFI materials (Fig. S14,† *vide infra*). This conclusion is also supported by the well-defined co-adsorption complexes of methanol and benzene or propene as displayed by the relatively small accessible ($\alpha$, $\beta$) area in Fig. 1g and h as compared to what was found for the AFI materials.

It can further be observed from Table 1 that propene is much more reactive towards methylation than benzene in H-ZSM-22, which is in line with what the MD based reactivity indices in Fig. 4 suggested and the experimental observation that the alkene cycle dominates in H-ZSM-22. Several experimental studies clearly pointed out that methanol conversion in H-ZSM-22 occurs through the alkene cycle and that aromatic HP species are not active.[73–75,77,78,125] Cui *et al.* reported that olefin growth occurs by subsequent methylation reactions and confirmed that growth of aromatic molecules was inhibited in the medium-sized pores of ZSM-22.[73] These findings are also clearly reflected in the free energy barriers for benzene and propene methylation reported in Table 1. Indeed, despite the relatively easy proton transfer reflected in the high probability to protonate methanol, the formation of favorable pre-reactive complexes for benzene methylation is hindered by spatial restrictions. In this respect, the results reported by Teketel *et al.* are worth mentioning as they claim to suppress the space demanding aromatics based MTO mechanism during methanol conversion in H-ZSM-22.[76–78] Analysis of the retained coke species after their MTO experiments showed that benzene derivatives are deactivating molecules during the reaction. Based on a single-event micro-kinetic modeling study, Kumar *et al.* also concluded that the alkene cycle dominates during methanol conversion in H-ZSM-23, which has a similar topology as H-ZSM-22.[31] Furthermore, the results for H-ZSM-22 in Table 1 show that methoxides are more reactive towards methylation than methanol, which can be understood in view of the less space demanding transition states during methylation by a methoxide as compared to physisorbed methanol (see Fig. 5).

Fig. 5 displays snapshots from the MTD simulations at 350 °C of benzene and propene methylation by methanol or a methoxide (a more extensive overview is given in Fig. S12†). For each snapshot, the values for $\alpha$ and $\beta$ at the top of the barrier are displayed and these values were indicated with a cross and circle in the histograms of Fig. 1 for a concerted and stepwise methylation step respectively. The entire evolution of the geometrical parameters $\alpha$, $\beta$, $\gamma$ and $\Delta$ as defined in Scheme 7 during reaction are displayed in Fig. S13.† We observed important reorientations of the guest molecules inside the one-dimensional pores during the barrier crossings (see videos in ESI†). In the AFI topology high $\alpha$ values and low $\beta$ values are adopted during the concerted methylation by methanol, whereas low $\alpha$ values and high $\beta$ values are required for methylation by a methoxide. It can be concluded that if a co-adsorption hotspot (white arrow in Fig. 1) occurs in the same ($\alpha$, $\beta$) value range as a required orientation for methylation by methanol (cross in Fig. 1) or a methoxide (circle in in Fig. 1), the system is very reactive towards a methylation. This is particularly the case for benzene and propene in H-SSZ-24 and propene in H-SAPO-5 (Fig. 1), which indeed all exhibit relatively low intrinsic free energy barriers in the range of 123–134 kJ mol$^{-1}$. This also fits the hypothesis based on the reactivity indices discussed in section 3.2. In the TON-structured H-ZSM-22 catalyst, the guest molecule orientations

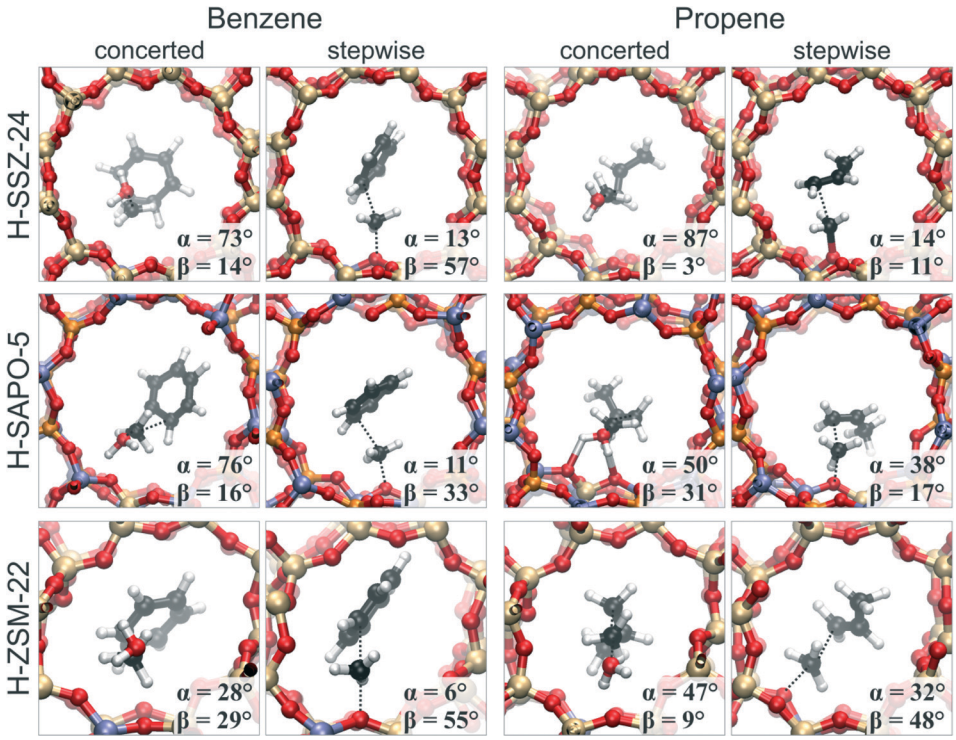


**Fig. 5** Snapshots of barrier crossings during MTD simulations of benzene methylation by methanol (concerted) or a methoxide (stepwise) at 350 °C in H-SSZ-24, H-SAPO-5 and H-ZSM-22 with indication of the $\alpha$ and $\beta$ value.

are much more confined and co-adsorption hotspots in Fig. 1g and h do not correspond to favorable orientations for methylation. In particular for the concerted benzene methylation in H-ZSM-22, an orientation has to be adopted that lies in a low probability region in Fig. 1g. It can thus be expected that in such case the reorientation of the hydrocarbons is an activated process and thus contributes to the relatively high free energy barrier for direct benzene methylation (151 ± 2 kJ mol$^{-1}$). The range in which the angles $\alpha$ and $\beta$ varied along the reaction paths sampled with the MTD simulations are presented in Fig. S14.†

A close inspection of the hydrocarbon orientation during simulation of concerted and stepwise methylation reactions revealed a correlation between co-adsorption hotspots prior to reaction, orientations at the top of the barrier and free energy barriers. Catalyst topology, acidity and reaction temperature each have a distinct impact on the reaction mechanism and kinetics and it seemed that this impact is not uniform for all reactions and differs for benzene and propene methylation.

**3.3.2 Additional guest molecules.** An additional set of MTD simulations of benzene methylation at 350 °C has been carried out, in which an additional methanol molecule was present around the BAS. Such additional protic molecule might play an active role during reactions in which proton transfer occurs, in this case the concerted methylation step and methoxide formation. The 2D FESs are displayed in Fig. S15.† The resulting free energy barriers and free energies of reaction are listed in Table 2.

Comparison between the results for one or two methanol molecules listed in Table 2 shows that the free energy barriers for the concerted methylation are all lowered by the presence of an additional protic molecule and the effect on the free energy barriers is more pronounced in H-SAPO-5 than in H-SSZ-24. In H-SSZ-24, methoxide formation is also facilitated by methanol; the assistance lowers the $\Delta G^{\ddagger}_{\text{step1}}$ values by 9 kJ mol$^{-1}$. This is however not the case in H-SAPO-5, in which methanol presence increases the free energy barrier for methoxide formation by 17 kJ mol$^{-1}$. This observation could be attributed to the low probability for methanol–methanol interactions in H-SAPO-5 in the absence of a hydrocarbon in the reactant state. Prior to reaction, the probability that the two methanol molecules interact *via* a hydrogen bond in H-SAPO-5 was less than 10%, whereas this was around 60% in H-SSZ-24. In H-SAPO-5 the assisting methanol

**Table 2** Free energy barriers and reaction energies in kJ mol$^{-1}$ for the concerted methylation of benzene ($\Delta G^{\ddagger}_{\text{concerted}}$) and methoxide formation ($\Delta G^{\ddagger}_{\text{step1}}$ and $\Delta G_{\text{r,step1}}$) by methanol assisted by an additional methanol molecule at 350 °C in H-SSZ-24 and H-SAPO-5. Reference values with 1 methanol molecule are given (cfr. Table 1)

| | | Concerted | Stepwise | |
|---|---|---|---|---|
| | 350 °C benzene | $\Delta G^{\ddagger}_{\text{concerted}}$ (kJ mol$^{-1}$) | $\Delta G^{\ddagger}_{\text{step1}}$ (kJ mol$^{-1}$) | $\Delta G_{\text{r,step1}}$ (kJ mol$^{-1}$) |
| H-SSZ-24 | 1 MeOH | 134 ± 3 | 160 ± 3 | 46 ± 4 |
| | 2 MeOH | 129 ± 5 | 151 ± 1 | 38 ± 1 |
| H-SAPO-5 | 1 MeOH | 156 ± 1 | 162 ± 3 | 3 ± 1 |
| | 2 MeOH | 142 ± 5 | 179 ± 1 | 43 ± 2 |

molecule mainly gets involved in the reaction once the reacting molecule is fully protonated, meaning that the enthalpic gain of the assistance is probably not high enough to compensate the associated entropic penalty.

The snapshots shown in Fig. 6 clearly show how 2 methanol molecules pair up to form a protonated hydrogen bonded cluster prior to reaction. However, we also observed reaction paths in which the additional methanol molecule did not play an active role (Fig. S16 and S17†). For the given conditions, it is thus not straightforward how such additional methanol molecule affects the kinetics and mechanism of benzene methylation. It can be expected that participation of an additional protic molecule introduces an additional entropic barrier; however an extended study is beyond the scope of this work.

## 4. Conclusions

In this study state-of-the-art advanced *ab initio* molecular dynamics (MD) techniques were used to assess the impact of reaction conditions and catalyst material on some crucial reaction steps of the zeolite-catalyzed methanol conversion process. In particular, the influence of catalyst topology and Brønsted acidity, reaction temperature and presence of an additional methanol molecule on the adsorption behavior and reaction mechanism and kinetics was investigated. The methylation of benzene and propene were selected as case studies as these are crucial reaction steps in the MTH chemistry. It is known that these reactions can occur either in a concerted or stepwise fashion, *i.e.* methanol directly transfers its methyl group to a hydrocarbon or the reaction goes through a framework-bound methoxide intermediate. The dynamical approach enables mimicking true reactions conditions as close as possible and studying the competition between two competing methylation mechanisms in an integrated fashion. The selectivity for one or the other mechanism has earlier been suggested to be entropy driven. A set of DFT-based MD and MTD simulations, which fully account for the mobility of the reacting species, has been performed on benzene and propene methylation in the AFI-structured H-SSZ-24 and H-SAPO-5 and the TON-structured H-ZSM-22 catalysts at 250 and 350 °C.

Our MD simulations point out that a vast number of co-adsorbed complexes can be formed for benzene and propene co-adsorbed with methanol, especially in AFI-structured materials. Nonetheless, some co-adsorption hotspots could be identified that correspond to the most probable co-adsorption complex. The location of these hotspots and thus the preferential orientation of benzene and propene in the pores were largely influenced by the catalyst topology and acidity, while temperature and presence of an additional methanol molecule only had a minor impact.

Additional insights on the reactivity towards methylation of these co-adsorption complexes were obtained by calculating the probability to protonate methanol and the probability to form favorable pre-reactive complexes for methylation. These indices and the insights based on the co-adsorption hotspots showed a clear correlation with the reactivity as calculated from the metadynamics simulations.

Next to the dynamical co-adsorption behavior and mobility of the guest molecules, the investigated process parameters also influenced the competition between a concerted and stepwise methylation mechanism. This competition was simulated by a large number of metadynamics simulations to obtain free energy barriers for every reaction step. At higher temperatures the stepwise pathway might become competitive with the concerted methylation, which indeed confirms the distinct entropic effects for both mechanisms. However, the competition between the two pathways is largely influenced by the specific material and hydrocarbon species. We observed in particular that for benzene methylation in H-SAPO-5 and H-ZSM-22 that a concerted methylation step and methoxide formation are nearly equally high activated. For a further assessment of this competition, the use of micro-kinetic models could be beneficial.

The influence of the catalyst's acid strength was assessed by comparison of results for two isostructural AFI materials H-SSZ-24 and H-SAPO-5, which have different framework compositions and thus acid strengths. In both materials slightly different co-adsorption complexes were found due to different interactions between the hydrocarbons and the zeolitic walls. In both materials, the concerted methylation dominates benzene and propene methylation, even at 350 °C. The impact of catalyst acidity on the free energies of activation does not seem to be uniform, but rather depends on the reaction type (concerted or stepwise) and the hydrocarbon undergoing the reaction, *i.e.* benzene or propene. As reported earlier in a combined experimental and theoretical study, benzene is more reactive towards methylation in H-SSZ-24,

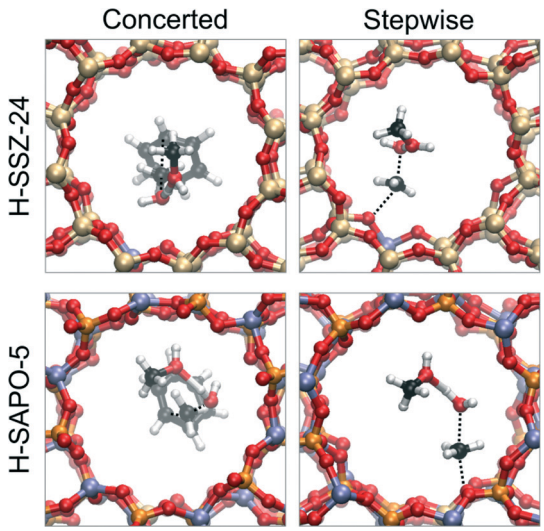


**Fig. 6** Snapshots of barrier crossings during MTD simulations of the concerted benzene methylation and first step of the stepwise pathway (methoxide formation) in H-SSZ-24 and H-SAPO-5 at 350 °C assisted by an additional methanol molecule.

whereas propene is more reactive in H-SAPO-5. This also corresponds with the experimental observation that the alkene mechanism dominates product formation during MTH reactions in H-SAPO-5, whereas aromatics are the most active HP species in H-SSZ-24.

Next, we also compared results for the AFI materials and TON catalyst to demonstrate the role of confinement on the methylation mechanism. Due to restricted mobility in the 10-ring channels, benzene exhibits a low reactivity towards methylation which can be related with its role as deactivating HP compound during methanol conversion. Once methoxides are formed, it is more probable that benzene gets methylated by a framework-bound methoxide due to a less space demanding transition state. Propene, which is assumed to be the dominant HP species in H-ZSM-22, indeed exhibits relatively low barriers for methylation from methanol and a methoxide. The higher reactivity of propene and low reactivity of benzene towards methylation are in line with experimental studies reporting that the medium-sized TON channels suppress the aromatics based reaction cycle and promote the alkene cycle during methanol conversion.

Finally, we addressed the impact of an additional methanol molecule on the kinetics of benzene methylation. The presence of such additional protic guest molecule mainly influences the ease of methanol protonation prior to reaction. We observed two types of reaction paths: paths in which the additional methanol actively participates and paths in which it doesn't. It seemed that the influence of such assistance on the free energy barriers of benzene methylation is not straightforward. Further dedicated studies on the impact of guest molecule loading and in particular the feed composition on the reaction mechanism are recommended from both an experimental and theoretical viewpoint.

Catalyst topology and acidity, reaction temperature and the presence of additional guest molecules, as included in this study each have a distinct impact on the reactivity of benzene and propene towards concerted or stepwise methylation. Our study clearly shows that obtaining profound insights into each of these factors is a complex task. However, by ingeniously selecting or varying each of the four factors, one is able to tune the reaction mechanism of an elementary zeolite-catalyzed reaction step. As we set focus on the complex dynamical behavior of the guest molecules in the pores, MD based techniques were the methods of choice in this study. As put forward in our recent review paper, theoretical models have matured substantially in the last decades. Chemical accuracy for barriers and kinetics was achieved for some particular case studies where the active site and mechanism was known, by using static yet very accurate theoretical methods. To deal with complexity at operating conditions complementary methods are needed as was shown in this paper. Future treatment of zeolite catalyzed reactions at operating conditions will need a close integration of different modeling tools at various length and time scales as was pointed out in ref. 12.

## Acknowledgements

We thank the Foundation of Scientific Research – Flanders (FWO), the Research Board of Ghent University, BELSPO (IAP P7/05) and the European Union's Horizon 2020 research and innovation programme (consolidator ERC grant agreement no 647755 – DYNPOR (2015-2020)). Computational resources and services were provided by the Stevin Supercomputer Infrastructure of Ghent University and by the Flemish Supercomputer Center (VSC), funded by the Hercules Foundation and the Flemish Government – department EWI.

## References

1 M. Guisnet and J. P. Gilson, *Zeolites for Cleaner Technologies*, Imperial College Press, London, 2002.
2 W. Vermeiren and J. P. Gilson, *Top. Catal.*, 2009, **52**, 1131–1161.
3 B. Yilmaz and U. Muller, *Top. Catal.*, 2009, **52**, 888–895.
4 J. Čejka, G. Centi, J. Perez-Pariente and W. J. Roth, *Catal. Today*, 2012, **179**, 2–15.
5 R. Chal, C. Gerardin, M. Bulut and S. van Donk, *ChemCatChem*, 2011, **3**, 67–81.
6 P. A. Jacobs, M. Dusselier and B. F. Sels, *Angew. Chem., Int. Ed.*, 2014, **53**, 8621–8626.
7 W. J. Roth, P. Nachtigall, R. E. Morris and J. Čejka, *Chem. Rev.*, 2014, **114**, 4807–4837.
8 M. B. J. Roeffaers, G. De Cremer, J. Libeert, R. Ameloot, P. Dedecker, A. J. Bons, M. Buckins, J. A. Martens, B. F. Sels, D. E. De Vos and J. Hofkens, *Angew. Chem., Int. Ed.*, 2009, **48**, 9285–9289.
9 B. M. Weckhuysen, *Angew. Chem., Int. Ed.*, 2009, **48**, 4910–4943.
10 I. L. C. Buurmans and B. M. Weckhuysen, *Nat. Chem.*, 2012, **4**, 873–886.
11 V. Van Speybroeck, K. De Wispelaere, J. Van der Mynsbrugge, M. Vandichel, K. Hemelsoet and M. Waroquier, *Chem. Soc. Rev.*, 2014, **43**, 7326–7357.
12 V. Van Speybroeck, K. Hemelsoet, L. Joos, M. Waroquier, R. G. Bell and C. R. A. Catlow, *Chem. Soc. Rev.*, 2015, **44**, 7044–7111.
13 U. Olsbye, S. Svelle, M. Bjørgen, P. Beato, T. V. W. Janssens, F. Joensen, S. Bordiga and K. P. Lillerud, *Angew. Chem., Int. Ed.*, 2012, **51**, 5810–5831.
14 J. Lefevere, S. Mullens, V. Meynen and J. Van Noyen, *Chem. Pap.*, 2014, **68**, 1143–1153.
15 B. V. Vora, T. L. Marker, P. T. Barger, H. R. Nilsen, S. Kvisle and T. Fuglerud, in *Studies in Surface Science and Catalysis*, ed. M. de Pontes, R. L. Espinoza, C. P. Nicolaides, J. H. Scholtz and M. S. Scurrell, Elsevier, 1997, vol. 107, pp. 87–98.
16 J. Q. Chen, A. Bozzano, B. Glover, T. Fuglerud and S. Kvisle, *Catal. Today*, 2005, **106**, 103–107.
17 H. Koempel and W. Liebner, in *Studies in Surface Science and Catalysis*, ed. F. B. Noronha, M. Schmal, E. Falabella and Sousa-Aguiar, Elsevier, 2007, vol. 167, pp. 261–267.

 

18 P. Tian, Y. Wei, M. Ye and Z. Liu, *ACS Catal.*, 2015, **5**, 1922–1938.
19 K. Hemelsoet, J. Van der Mynsbrugge, K. De Wispelaere, M. Waroquier and V. Van Speybroeck, *ChemPhysChem*, 2013, **14**, 1526–1545.
20 M. Stöcker, *Microporous Mesoporous Mater.*, 1999, **29**, 3–48.
21 S. Ilias and A. Bhan, *ACS Catal.*, 2013, **3**, 18–31.
22 S. Svelle, U. Olsbye, F. Joensen and M. Bjørgen, *J. Phys. Chem. C*, 2007, **111**, 17981–17984.
23 S. Svelle, F. Joensen, J. Nerlov, U. Olsbye, K. P. Lillerud, S. Kolboe and M. Bjørgen, *J. Am. Chem. Soc.*, 2006, **128**, 14770–14771.
24 M. Bjørgen, F. Joensen, K. P. Lillerud, U. Olsbye and S. Svelle, *Catal. Today*, 2009, **142**, 90–97.
25 D. Chen, K. Moljord and A. Holmen, *Microporous Mesoporous Mater.*, 2012, **164**, 239–250.
26 U. Olsbye, S. Svelle, K. P. Lillerud, Z. H. Wei, Y. Y. Chen, J. F. Li, J. G. Wang and W. B. Fan, *Chem. Soc. Rev.*, 2015, **44**, 7155–7176.
27 K. P. F. Janssen, G. De Cremer, R. K. Neely, A. V. Kubarev, J. Van Loon, J. A. Martens, D. E. De Vos, M. B. J. Roeffaers and J. Hofkens, *Chem. Soc. Rev.*, 2014, **43**, 990–1006.
28 J. Van der Mynsbrugge, M. Visur, U. Olsbye, P. Beato, M. Bjørgen, V. Van Speybroeck and S. Svelle, *J. Catal.*, 2012, **292**, 201–212.
29 S. Svelle, M. Visur, U. Olsbye, Saepurahman and M. Bjørgen, *Top. Catal.*, 2011, **54**, 897–906.
30 P. Kumar, J. W. Thybaut, S. Svelle, U. Olsbye and G. B. Marin, *Ind. Eng. Chem. Res.*, 2013, **52**, 1491–1507.
31 P. Kumar, J. W. Thybaut, S. Teketel, S. Svelle, P. Beato, U. Olsbye and G. B. Marin, *Catal. Today*, 2013, **215**, 224–232.
32 R. Y. Brogaard, R. Henry, Y. Schuurman, A. J. Medford, P. G. Moses, P. Beato, S. Svelle, J. K. Nørskov and U. Olsbye, *J. Catal.*, 2014, **314**, 159–169.
33 S. M. Alwahabi and G. F. Froment, *Ind. Eng. Chem. Res.*, 2004, **43**, 5098–5111.
34 J. Van der Mynsbrugge, K. Hemelsoet, M. Vandichel, M. Waroquier and V. Van Speybroeck, *J. Phys. Chem. C*, 2012, **116**, 5499–5508.
35 S. Svelle, C. Tuma, X. Rozanska, T. Kerber and J. Sauer, *J. Am. Chem. Soc.*, 2009, **131**, 816–825.
36 V. Van Speybroeck, J. Van der Mynsbrugge, M. Vandichel, K. Hemelsoet, D. Lesthaeghe, A. Ghysels, G. B. Marin and M. Waroquier, *J. Am. Chem. Soc.*, 2011, **133**, 888–899.
37 G. Piccini, M. Alessio, J. Sauer, Y. C. Zhi, Y. Liu, R. Kolvenbach, A. Jentys and J. A. Lercher, *J. Phys. Chem. C*, 2015, **119**, 6128–6137.
38 G. Piccini and J. Sauer, *J. Chem. Theory Comput.*, 2013, **9**, 5038–5045.
39 T. Bučko, *J. Phys.: Condens. Matter*, 2008, **20**, 9.
40 B. Ensing, A. Laio, M. Parrinello and M. L. Klein, *J. Phys. Chem. B*, 2005, **109**, 6676–6687.
41 L. Benco, T. Bučko and J. Hafner, *J. Catal.*, 2011, **277**, 104–116.
42 T. Bučko, L. Benco, O. Dubay, C. Dellago and J. Hafner, *J. Chem. Phys.*, 2009, **131**, 11.
43 T. Bučko, L. Benco, J. Hafner and J. G. Angyan, *J. Catal.*, 2011, **279**, 220–228.
44 T. Bučko and J. Hafner, *J. Catal.*, 2015, **329**, 32–48.
45 F. Göltl and J. Hafner, *Microporous Mesoporous Mater.*, 2013, **166**, 176–184.
46 T. Jiang, F. Göltl, R. E. Bulo and P. Sautet, *ACS Catal.*, 2014, **4**, 2351–2358.
47 J. Gomes, M. Head-Gordon and A. T. Bell, *J. Phys. Chem. C*, 2014, **118**, 21409–21419.
48 P. M. Zimmerman, D. C. Tranca, J. Gomes, D. S. Lambrecht, M. Head-Gordon and A. T. Bell, *J. Am. Chem. Soc.*, 2012, **134**, 19468–19476.
49 K. De Wispelaere, B. Ensing, A. Ghysels, E. J. Meijer and V. Van Speybroeck, *Chem. – Eur. J.*, 2015, **21**, 9385–9396.
50 A. Ghysels, S. L. C. Moors, K. Hemelsoet, K. De Wispelaere, M. Waroquier, G. Sastre and V. Van Speybroeck, *J. Phys. Chem. C*, 2015, **119**, 23721–23734.
51 S. L. C. Moors, K. De Wispelaere, J. Van der Mynsbrugge, M. Waroquier and V. Van Speybroeck, *ACS Catal.*, 2013, **3**, 2556–2567.
52 J. Van der Mynsbrugge, S. L. C. Moors, K. De Wispelaere and V. Van Speybroeck, *ChemCatChem*, 2014, **6**, 1906–1918.
53 M. Westgård Erichsen, K. De Wispelaere, K. Hemelsoet, S. L. C. Moors, T. Deconinck, M. Waroquier, S. Svelle, V. Van Speybroeck and U. Olsbye, *J. Catal.*, 2015, **328**, 186–196.
54 S. H. Zheng and J. Pfaendtner, *Mol. Simul.*, 2015, **41**, 55–72.
55 K. De Wispelaere, K. Hemelsoet, M. Waroquier and V. Van Speybroeck, *J. Catal.*, 2013, **305**, 76–80.
56 D. Lesthaeghe, B. De Sterck, V. Van Speybroeck, G. B. Marin and M. Waroquier, *Angew. Chem., Int. Ed.*, 2007, **46**, 1311–1314.
57 D. M. McCann, D. Lesthaeghe, P. W. Kletnieks, D. R. Guenther, M. J. Hayman, V. Van Speybroeck, M. Waroquier and J. F. Haw, *Angew. Chem., Int. Ed.*, 2008, **47**, 5179–5182.
58 C. M. Wang, Y. D. Wang, Z. K. Xie and Z. P. Liu, *J. Phys. Chem. C*, 2009, **113**, 4584–4591.
59 I. M. Hill, S. Al Hashimi and A. Bhan, *J. Catal.*, 2012, **285**, 115–123.
60 S. Svelle, P. A. Ronning and S. Kolboe, *J. Catal.*, 2004, **224**, 115–123.
61 S. Svelle, P. O. Ronning, U. Olsbye and S. Kolboe, *J. Catal.*, 2005, **234**, 385–400.
62 V. Van Speybroeck, K. Hemelsoet, K. De Wispelaere, Q. Qian, J. Van der Mynsbrugge, B. De Sterck, B. M. Weckhuysen and M. Waroquier, *ChemCatChem*, 2013, **5**, 173–184.
63 S. Al-Khattaf, S. A. Ali, A. M. Aitani, N. Zilkova, D. Kubicka and J. Čejka, *Catal. Rev.: Sci. Eng.*, 2014, **56**, 333–402.
64 S. Svelle and M. Bjørgen, *J. Phys. Chem. A*, 2010, **114**, 12548–12554.
65 J. Van der Mynsbrugge, J. De Ridder, K. Hemelsoet, M. Waroquier and V. Van Speybroeck, *Chem. – Eur. J.*, 2013, **19**, 11568–11576.
66 T. Maihom, B. Boekfa, J. Sirijaraensre, T. Nanok, M. Probst and J. Limtrakul, *J. Phys. Chem. C*, 2009, **113**, 6654–6662.

67 H. Yamazaki, H. Shima, H. Imai, T. Yokoi, T. Tatsumi and J. N. Kondo, *Angew. Chem., Int. Ed.*, 2011, **50**, 1853–1856.
68 I. M. Hill, Y. S. Ng and A. Bhan, *ACS Catal.*, 2012, **2**, 1742–1748.
69 I. Hill, A. Malek and A. Bhan, *ACS Catal.*, 2013, **3**, 1992–2001.
70 S. Ilias and A. Bhan, *J. Catal.*, 2012, **290**, 186–192.
71 S. Svelle, S. Kolboe, O. Swang and U. Olsbye, *J. Phys. Chem. B*, 2005, **109**, 12874–12878.
72 Y. Y. Chu, X. Y. Sun, X. F. Yi, L. H. Ding, A. M. Zheng and F. Deng, *Catal. Sci. Technol.*, 2015, **5**, 3507–3517.
73 Z. M. Cui, Q. Liu, Z. Ma, S. W. Bian and W. G. Song, *J. Catal.*, 2008, **258**, 83–86.
74 J. Z. Li, Y. X. Wei, G. Y. Liu, Y. Qi, P. Tian, B. Li, Y. L. He and Z. M. Liu, *Catal. Today*, 2011, **171**, 221–228.
75 J. Z. Li, Y. X. Wei, Y. Qi, P. Tian, B. Li, Y. L. He, F. X. Chang, X. D. Sun and Z. M. Liu, *Catal. Today*, 2011, **164**, 288–292.
76 S. Teketel, U. Olsbye, K. P. Lillerud, P. Beato and S. Svelle, *Microporous Mesoporous Mater.*, 2010, **136**, 33–41.
77 S. Teketel, W. Skistad, S. Benard, U. Olsbye, K. P. Lillerud, P. Beato and S. Svelle, *ACS Catal.*, 2012, **2**, 26–37.
78 S. Teketel, S. Svelle, K. P. Lillerud and U. Olsbye, *ChemCatChem*, 2009, **1**, 78–81.
79 B. P. C. Hereijgers, F. Bleken, M. H. Nilsen, S. Svelle, K. P. Lillerud, M. Bjørgen, B. M. Weckhuysen and U. Olsbye, *J. Catal.*, 2009, **264**, 77–87.
80 M. Bjørgen, S. Akyalcin, U. Olsbye, S. Benard, S. Kolboe and S. Svelle, *J. Catal.*, 2010, **275**, 170–180.
81 M. Bjørgen, U. Olsbye, D. Petersen and S. Kolboe, *J. Catal.*, 2004, **221**, 1–10.
82 M. Westgård Erichsen, S. Svelle and U. Olsbye, *Catal. Today*, 2013, **215**, 216–223.
83 C. Wang, B. Li, Y. Wang and Z. Xie, *J. Energy Chem.*, 2013, **22**, 914–918.
84 A. F. Combariza, G. Sastre and A. Corma, *J. Phys. Chem. C*, 2011, **115**, 875–884.
85 Database of zeolite structures, http://www.iza-structure.org/databases/.
86 F. Bleken, M. Bjørgen, L. Palumbo, S. Bordiga, S. Svelle, K. P. Lillerud and U. Olsbye, *Top. Catal.*, 2009, **52**, 218–228.
87 M. Westgård Erichsen, S. Svelle and U. Olsbye, *J. Catal.*, 2013, **298**, 94–101.
88 X. Y. Sun, S. Mueller, Y. Liu, H. Shi, G. L. Haller, M. Sanchez-Sanchez, A. C. van Veen and J. A. Lercher, *J. Catal.*, 2014, **317**, 185–197.
89 E. Borodina, F. Meirer, I. Lezcano-González, M. Mokhtar, A. M. Asiri, S. A. Al-Thabaiti, S. N. Basahel, J. Ruiz-Martínez and B. M. Weckhuysen, *ACS Catal.*, 2015, **5**, 992–1003.
90 J. H. Ahn, B. Temel and E. Iglesia, *Angew. Chem., Int. Ed.*, 2009, **48**, 3814–3816.
91 D. A. Simonetti, J. H. Ahn and E. Iglesia, *J. Catal.*, 2011, **277**, 173–195.
92 A. J. Jones and E. Iglesia, *Angew. Chem., Int. Ed.*, 2014, **53**, 12177–12181.
93 R. Gounder and E. Iglesia, *Acc. Chem. Res.*, 2012, **45**, 229–238.
94 J. A. Brennan, S. J. Lucki and H. J. Schoennagel, Catalysts for the conversion of methanol to ethylene plus gasoline, *US Pat.*, 4480145, 1984.
95 W. W. Kaeding and S. A. Butter, Conversion of methanol and dimethyl ether, *US Pat.*, 3911041, 1975.
96 A. N. Mlinar, P. M. Zimmerman, F. E. Celik, M. Head-Gordon and A. T. Bell, *J. Catal.*, 2012, **288**, 65–73.
97 J. Hutter, M. Iannuzzi, F. Schiffmann and J. VandeVondele, *Wiley Interdiscip. Rev.: Comput. Mol. Sci.*, 2014, **4**, 15–25.
98 J. VandeVondele, M. Krack, F. Mohamed, M. Parrinello, T. Chassaing and J. Hutter, *Comput. Phys. Commun.*, 2005, **167**, 103–128.
99 G. Lippert, J. Hutter and M. Parrinello, *Theor. Chem. Acc.*, 1999, **103**, 124–140.
100 G. Lippert, J. Hutter and M. Parrinello, *Mol. Phys.*, 1997, **92**, 477–487.
101 K. Yang, J. J. Zheng, Y. Zhao and D. G. Truhlar, *J. Chem. Phys.*, 2010, **132**, 10.
102 S. Goedecker, M. Teter and J. Hutter, *Phys. Rev. B: Condens. Matter Mater. Phys.*, 1996, **54**, 1703–1710.
103 S. Grimme, J. Antony, S. Ehrlich and H. Krieg, *J. Chem. Phys.*, 2010, **132**, 19.
104 D. Frenkel and B. Smit, *Understanding Molecular Simulations*, Academic press, Elsevier, 2nd edn, 2002.
105 G. J. Martyna, D. J. Tobias and M. L. Klein, *J. Chem. Phys.*, 1994, **101**, 4177–4189.
106 A. Laio and F. L. Gervasio, *Rep. Prog. Phys.*, 2008, **71**, 22.
107 P. Tiwary and M. Parrinello, *Phys. Rev. Lett.*, 2013, **111**, 5.
108 L. Goerigk and S. Grimme, *Phys. Chem. Chem. Phys.*, 2011, **13**, 6670–6688.
109 Y. Zhao and D. G. Truhlar, *J. Phys. Chem. C*, 2008, **112**, 6860–6868.
110 Y. Zhao and D. G. Truhlar, *Theor. Chem. Acc.*, 2008, **120**, 215–241.
111 Y. Zhao and D. G. Truhlar, *J. Chem. Theory Comput.*, 2008, **4**, 1849–1868.
112 Y. Zhao and D. G. Truhlar, *Acc. Chem. Res.*, 2008, **41**, 157–167.
113 J. D. Chai and M. Head-Gordon, *Phys. Chem. Chem. Phys.*, 2008, **10**, 6615–6620.
114 J. Wellendorff, K. T. Lundgaard, A. Møgelhøj, V. Petzold, D. D. Landis, J. K. Nørskov, T. Bligaard and K. W. Jacobsen, *Phys. Rev. B: Condens. Matter Mater. Phys.*, 2012, **85**, 235149.
115 S. B. McCullen, P. T. Reischman and D. H. Olson, *Zeolites*, 1993, **13**, 640–644.
116 C. O. Arean, M. R. Delgado, P. Nachtigall, H. V. Thang, M. Rubes, R. Bulanek and P. Chlubna-Eliasova, *Phys. Chem. Chem. Phys.*, 2014, **16**, 10129–10141.
117 E. G. Derouane, J. C. Vedrine, R. R. Pinto, P. M. Borges, L. Costa, M. Lemos, F. Lemos and F. R. Ribeiro, *Catal. Rev.: Sci. Eng.*, 2013, **55**, 454–515.
118 C. Lo, C. A. Giurumescu, R. Radhakrishnan and B. L. Trout, *Mol. Phys.*, 2004, **102**, 281–288.
119 J. Sauer, M. Sierka and F. Haase, in *Transitions State Modeling for Catalysis*, ed. K. Morokuma and D. G. Truhlar, American Chemical Society, Washington DC, 1999, pp. 358–367.

 

120 F. Haase, J. Sauer and J. Hutter, *Chem. Phys. Lett.*, 1997, **266**, 397–402.
121 J. D. Gale, R. Shah, M. C. Payne, I. Stich and K. Terakura, *Catal. Today*, 1999, **50**, 525–532.
122 I. Stich, J. D. Gale, K. Terakura and M. C. Payne, *J. Am. Chem. Soc.*, 1999, **121**, 3292–3302.
123 F. Göltl, A. Gruneis, T. Bučko and J. Hafner, *J. Chem. Phys.*, 2012, **137**, 17.
124 J. Macht, R. T. Carr and E. Iglesia, *J. Am. Chem. Soc.*, 2009, **131**, 6554–6565.
125 Q. Wang, Z. M. Cui, C. Y. Cao and W. G. Song, *J. Phys. Chem. C*, 2011, **115**, 24987–24992.